LABORATORY INVESTIGATION OF CHEMICAL AND PHYSICAL PROPERTIES OF SOOT-CONTAINING AEROSOLS

A Dissertation

by

DAN ZHANG

Submitted to the Office of Graduate Studies of
Texas A&M University
in partial fulfillment of the requirements for the degree of

DOCTOR OF PHILOSOPHY

May 2006

Major Subject: Atmospheric Sciences

LABORATORY INVESTIGATION OF CHEMICAL AND PHYSICAL PROPERTIES OF SOOT-CONTAINING AEROSOLS

A Dissertation

by

DAN ZHANG

Submitted to the Office of Graduate Studies of
Texas A&M University
in partial fulfillment of the requirements for the degree of

DOCTOR OF PHILOSOPHY

Approved by:

Chair of Committee, Renyi Zhang
Committee Members, Don R. Collins
Robert A. Duce
Simon W. North
Head of Department, Richard E. Orville

May 2006

Major Subject: Atmospheric Sciences

ABSTRACT

Laboratory Investigation of Chemical and Physical Properties of Soot-Containing Aerosols. (May 2006)

Dan Zhang, B.S., Fudan University, China;

M.S., Texas A&M University

Chair of Advisory Committee: Dr. Renyi Zhang

Soot particles released from fossil fuel combustion and biomass burning have a large impact on the regional/global climate by altering the atmospheric radiative properties and by serving as cloud condensation nuclei (CCN). However, the exact forcing is affected by the mixing of soot with other aerosol constituents, such as sulfuric acid. In this work, experimental studies have been carried out focusing on three integral parts: (1) heterogeneous uptake of sulfuric acid on soot; (2) hygroscopic growth of H_2SO_4-coated soot aerosols; (3) effect of H_2SO_4 coating on scattering and extinction properties of soot particles. A low-pressure laminar-flow reactor, coupled to ion drift-chemical ionization mass spectrometry (ID-CIMS) detection, is used to study uptake coefficients of H_2SO_4 on combustion soot. The results suggest that uptake of H_2SO_4 takes place efficiently on soot particles, representing an important route to convert hydrophobic soot to hydrophilic aerosols. A tandem differential mobility analyzing (TDMA) system is employed to determine the hygroscopicity of freshly generated soot in the presence of H_2SO_4 coating. It is found that fresh soot particles are highly hydrophobic, while coating of H_2SO_4 significantly facilitates water uptake on soot even at sub-saturation relative humidities. The results indicate that aged soot particles in the

atmosphere can potentially be an efficient source of CCN. Scattering and extinction coefficient measurements of the soot-H_2SO_4 mixed particles are conducted using a three-wavelength Nephelometer and a multi-path extinction cell. Coating of H_2SO_4 is found to increase the single scattering albedo (SSA) of soot particles which has impact on the aerosol direct radiative effect. Other laboratory techniques such as transmission electron microscopy (TEM) and Fourier transform infrared spectrometry (FTIR) are utilized to examine the morphology and chemical composition of the soot-H_2SO_4 particles.

This work provides critical information concerning the heterogeneous interaction of soot and sulfuric acid, and how their mixing affects the hygroscopic and optical properties of soot. The results will improve our ability to model and assess the soot direct and indirect forcing and hence enhance our understanding of the impact of anthropogenic activities on the climate.

TABLE OF CONTENTS

Page

LIST OF FIGURES

FIGURE Page

LIST OF TABLES

CHAPTER I

INTRODUCTION

Atmospheric aerosols play an important role in regulating the solar radiation intake in the Earth-atmosphere system. The aerosol direct effect on the climate lies in the absorption and scattering of solar radiation by aerosols, leading to warming or cooling of the atmosphere. The aerosol indirect effect is caused by aerosols that act as cloud condensation nuclei (CCN) and alter the cloud forming properties. There are two types of aerosol indirect effects: enhanced cloud albedo, the first indirect effect, and suppressed rain, the second indirect effect. Figure 1-1, taken from the report by the Intergovernmental Panel on Climate Change (IPCC) in 2001, shows the global radiative forcings due to both natural and anthropogenic factors since the pre-industrial period. The figure indicates that currently there are still large uncertainties on the aerosol direct and indirect radiative effects and our understanding of these effects are very low.

Soot particles, formed as a result of incomplete combustion of fossil and bio-fuels, and outdoor biomass burning, have an average global source estimated to be as high as 24 Tg yr^{-1} [*Penner et al.*, 1993]. They are of special interest because of their significant impacts on global radiative balance and climate, both directly by absorbing solar and terrestrial radiation [*Horvath*, 1993] and indirectly by serving as CCN [*Jensen and Toon*, 1997]. Light absorption in the visible range is primarily due to soot particles. Once emitted into the atmosphere, soot particles are subjected to several aging processes, such as adsorption and condensation of gaseous species on soot surfaces,

---

This thesis follows the style and format of the *Journal of Geophysical Research*.

coagulation of soot with other pre-existing aerosol constituents, and oxidation of soot by various atmospheric species. Internally mixed soot particles are also produced from burning fuels with sulfur-containing addictives. The hygroscopicity and optical properties of soot are likely altered during the aging processes, leading to potential influence in the direct and indirect radiative forcings of soot.

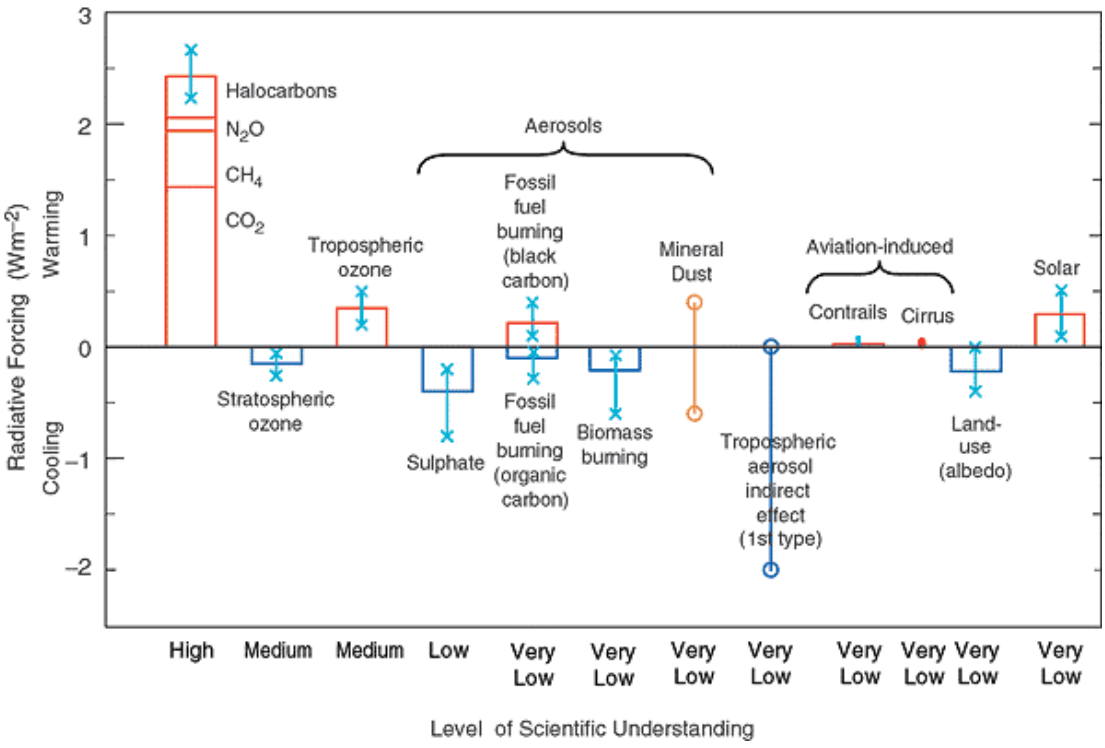

Figure 1-1. Global, annual-mean radiative forcings due to a number of agents for the period from pre-industrial (1750) to 2000. [*IPCC*, 2001]

Numerous efforts have been made in laboratory, field, and modeling studies to determine the sources, distribution, heterogeneous reactivity, and radiative properties of

soot in the atmosphere. However, there still exist several key areas that remain uncertain and unexplored. One major difficulty in assessing the radiative forcing of soot lies in inadequate information of the dependence of cloud-forming and optical properties on the mixing of soot with other aerosol constituents. Field and laboratory investigations revealed that aircraft engine soot was a primary contributor to contrail nuclei due to the impurities containing soluble sulfates and organics [*Karcher et al.*, 1996; *Popovicheva et al.*, 2004]. Recent model calculations indicated that soot could exert higher "positive" direct radiative forcing when associated with other scattering aerosols, e.g., sulfate, nitrate, and organic carbon [*Jacobson*, 2000]. Because of the high positive forcing of soot mixtures, it was suggested that the warming effect from black carbon may nearly balance the net cooling effect of other anthropogenic aerosol constituents [*Jacobson*, 2001].

Despite the ample field measurements on the mixing state of soot and modeling studies of its effect on the radiative forcing [e.g., *Chylek and Wong*., 1995; *Fuller et al*., 1999; *Lesins et al.*, 2002], little has been done in the laboratory to investigate the interaction between soot and other aerosol constituents and the impact of soot mixing state on its hygroscopic and optical properties. To date only a few laboratory studies during the European AIDA Soot Aerosol Campaign 1999 have investigated the hygroscopic and optical properties of soot mixed with ammonium sulfate and secondary organic aerosols from α-pinene ozonolysis in chamber experiments [*Saathoff et al*., 2003a; *Schnaiter et al.,* 2003]. No laboratory study is available on the mixing of soot with other important aerosols, such as sulfuric acid in a controlled manner. In addition,

although studies have been carried out to determine the uptake coefficients of nitrogen oxides and nitric acid on soot surface [e.g., *Longfellow et al.*, 1999; *Longfellow et al.*, 2000; *Prince et al.*, 2002], there lacks experimental data on the heterogeneous reactivity of soot with other gaseous aerosol precursors, especially sulfuric acid, which provides crucial information in understanding the aging process of soot in industrial areas.

This work involves laboratory studies of heterogeneous interaction of soot with an important aerosol constituent, sulfuric acid, and the hygroscopicity and optical properties of the mixed soot under controlled experimental conditions. This research provides valuable information concerning the interaction of soot with sulfuric acid, and the influence of this interaction on soot hygroscopicity and optical properties. The results hence enhance our understanding of the impact of soot-containing particles on both direct and indirect climate forcings.

This dissertation consists of five chapters. An overview of atmospheric soot particles, their aging processes and their radiative effects is given in Chapter I. The three parts of studies included in the work are also outlined. Chapters II, III, and IV each consists of four sub-sections: introduction, experimental section, results and discussions, and summary. Chapter II focuses on the study of the heterogeneous interaction of sulfuric acid with soot. Chapter III concentrates on the hygroscopic growth of both fresh soot and soot that is coated with sulfuric acid. Chapter IV presents the scattering and extinction measurements of soot-containing aerosols. Finally, concluding remarks are given in Chapter V.

CHAPTER II

HETEROGENEOUS INTERACTION OF SULFURIC ACID WITH SOOT

2.1. Introduction

Atmospheric aerosols play an important role in regulating cloud formation and solar radiation intake in the Earth-atmosphere system. Soot particles are of special interest because of their role in atmospheric heterogeneous reactions, cloud formation, and global radiative balance and climate. The aerosol direct effect lies in the large absorbing efficiency of solar and terrestrial radiation by soot [*Horvath*, 1993]. In addition, they may serve as cloud condensation nuclei (CCN) [*Jensen and Toon*, 1997]. In particular, the activation of soot particles as CCN is thought to be enhanced by the uptake of water-soluble inorganic species such as H_2SO_4 and HNO_3 [*Hallett et al*., 1989; *Brown*, 1996; *Schumann et al.*, 1996]. Sulfuric acid plays a key role in atmospheric new particle formation. Gaseous H_2SO_4 in the atmosphere is produced by the oxidation of SO_2, which is from either direct industrial and automobile emission or oxidation of reduced biogenic sulfur compounds. H_2SO_4 in the gas phases can have two fates: homogeneous nucleation with H_2O, NH_3, or organic vapors leading to new particle formation [e.g. *Weber et al.*, 1996; *Viisanen et al.*, 1997; *Zhang et al.*, 2004], and heterogeneous scavenging by preexisting aerosols resulting in particle growth. In the latter case, soot particles provide heterogeneous surfaces for H_2SO_4 uptake in the urban and regional atmosphere, forming internally mixed aerosols. Because of the abundance and the climatic impact of soot and H_2SO_4 in the atmosphere, it is of importance to

understand their heterogeneous interaction in order to provide quantitative information for current models involving aerosol microphysics and aerosol/cloud interaction.

Numerous efforts have been made in laboratory, field, and modeling studies to determine the sources, distribution, heterogeneous reactivity, and radiative properties of soot in the atmosphere. The radiative properties of soot are largely affected by its mixing with other atmospheric species. Typically, the mixing state of soot in the atmosphere is characterized by two extreme scenarios: soot partially or entirely coated within other organic/inorganic constituents (internally mixed) and distinct soot particles mixed externally with other aerosol types (externally mixed). Model calculations have indicated that soot could exert higher "positive" direct radiative forcing when associated with other scattering aerosols, e.g., sulfate, nitrate, and organic carbon [*Jacobson*, 2000]. In addition, internal mixture of soot with other aerosol ingredients appears significantly more absorptive than the external mixture counterpart [*Jacobson*, 2000]. Because of the high positive forcing of soot mixtures, it has been suggested that the warming effect from black carbon may nearly balance the net cooling effect of other anthropogenic aerosol constituents [*Jacobson*, 2001].

Several field measurements have been carried out to investigate the mixing state of atmospheric soot particles in urban and rural areas. For example, *Hasegawa and Ohta* [2002] examined samples of individual soot-containing particles using the dialysis of water-soluble components and electron microscopy. Size distribution and morphology of ambient mixed soot particles were studied using differential mobility analyzer and transmission electron microscopy [*Okada and Heintzenberg*, 2003]. A recent study by

Mallet and co-workers [2004] employed a novel approach to estimate the mixing state of soot in urban areas by comparing the measured single scattering albedo with values calculated for both internal and external mixing cases. Field measurement results revealed that soot particles in urban area were mostly externally mixed, while internal mixtures were more prevalent at rural sites.

Numerous experiments have been performed in the laboratory to investigate uptake of certain atmospheric species on soot, such as water [e.g., *Seisel et al.*, 2004; *Alcala-Jornod and Rossi*, 2004], ozone [e.g., *Lelievre et al.*, 2004a] and nitrogen-containing compounds [e.g., *Choi and Leu*, 1998; *Longfellow et al.*, 1999; *Longfellow, et al.*, 2000; *Al-Abadleh and Grassian*, 2000; *Prince et al.*, 2002; *Aubin and Abbatt*, 2003]. The reported uptake coefficients of the various chemical species on soot vary by several orders of magnitude, depending on the soot type, soot deactivation process due to exposure to the reactant, and concentrations of the gaseous species used. Other previous studies have reported measurements of H_2SO_4 mass accommodation and uptake coefficient on aqueous H_2SO_4 as well as sea salt aerosol surfaces [*Poschl et al.*, 1998; *ten Brink*, 1998; *Jefferson et al.*, 1997]. Despite the considerable interest in the interaction between soot and H_2SO_4, to date no kinetic data are available on uptake of gas-phase H_2SO_4 on soot, which is crucial in understanding the role of soot particles in cloud formation, radiative transfer, and heterogeneous chemistry.

In this chapter, we report measurements of the uptake coefficients of H_2SO_4 on the surfaces of soot generated from methane, hexane and kerosene combustion. The kinetic experiments are conducted with a low-pressure, coated-wall laminar flow reactor

apparatus equipped with ion drift - chemical ionization mass spectrometry (ID-CIMS). We also investigate the potential of soot deactivation by exposing soot to H_2SO_4 over an extended time period. A Fourier transform infrared spectrometer (FTIR) is employed to collect IR spectra of soot and soot-H_2SO_4 aerosols to further characterize the interaction of H_2SO_4 with soot.

2.2. Experimental Section

2.2.1. Heterogeneous Uptake of Sulfuric Acid on Soot. The uptake experiments were conducted in a low-pressure, coated-wall laminar flow reactor coupled to an ion drift - chemical ionization mass spectrometry (ID-CIMS) system shown schematically in Figure 2-1. The flow reactor was a cylindrical Pyrex glass tube of 35 cm in length. Soot produced from burning three different types of fuels (methane, hexane, and kerosene) was evenly deposited on the inner wall of a 20 cm long, 1.65 cm i.d Pyrex tube suspended above the flame, which was then inserted inside the flow reactor. The total mass of soot deposited was measured to be in the range of 1-10 mg for all experiments with a typical amount of 2 mg. An O-ring seal valve was installed between the flow reactor and the ID-CIMS so that replacement of the soot-coated tube was easily facilitated without breaking the vacuum of the mass spectrometer system. The methane flame was produced with a Santoro-type co-flow laminar diffusion burner, which consisted of two concentric tubes for fuel and air to flow through the inner and outer tubes, respectively [*Santoro et al.*, 1983]. The kerosene and hexane flames were generated using a commercial alcohol burner. A N_2 carrier gas flow of ~100 sccm was passed through a bubbler containing ~1ml of commercial 96 wt % H_2SO_4. Sulfuric acid

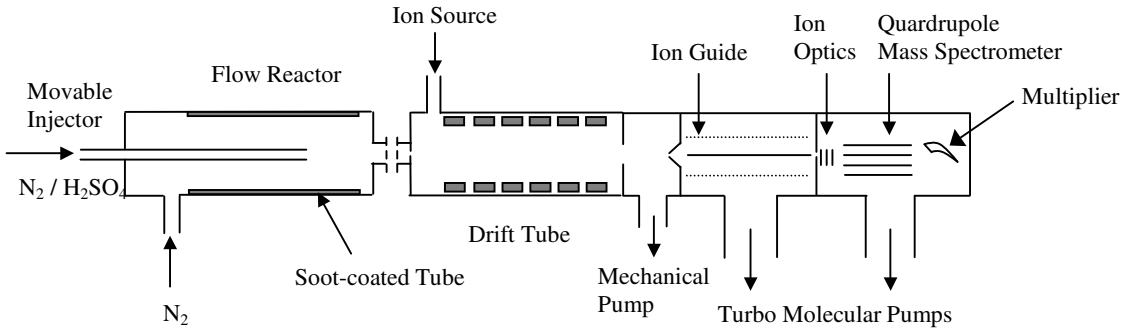

Figure 2-1. Schematic representation of the flow reactor - ID-CIMS system setup.

was introduced into the flow reactor through a central movable injector. The H_2SO_4 partial pressure in the flow reactor was estimated to be on the order of 10^{-7} to 10^{-8} Torr using the ID-CIMS method [*Zhang et al.*, 2004; *Fortner et al.*, 2004]. Dry N_2 entrained into the reactor *via* a side port near the entrance was used as the main carrier gas, reaching a flow velocity characteristic of laminar flow conditions (i.e., the Reynolds number $Re = 2au\rho/\mu < 2000$, where a is the internal radius of the flow reactor in cm, ρ the density of the gas in g cm^{-3}, u the flow velocity in cm s^{-1}, and μ the absolute viscosity of the gas in g cm^{-1} s^{-1}). The Reynolds number was in the range of 30-60 for all experiments in this study. All carrier flows were monitored with calibrated electronic mass flow meters (Millipore Tylan 260 Series). The flow reactor operated at low pressures (about 1-2 Torr) and room temperature, with typical flow velocities of 1600-2200 cm s^{-1}. All experiments were performed at 298 ± 2 K.

Details of the ID-CIMS instrumentation were described previously [*Fortner et al.*, 2004]. Briefly, the ID-CIMS system consisted of an ion source, a drift tube, and a chemical ionization mass spectrometer (CIMS). Gas flow from the flow reactor was entrained directly into the drift tube region. A custom-made corona discharge was used as the ion source. For H_2SO_4 detection, nitrogen mixed with SF_6 at the ppm level was admitted through the corona charge while a high negative voltage (-5kV) was applied to produce SF_6^- reagent ions. The primary ion-molecule reaction between H_2SO_4 and SF_6^- occurred at a rate near the collision limit, leading to the formation of HSO_4^- (*m/e* = 97) [*Poschl et al.*, 1998]. The drift tube was constructed with a 50 cm length Pyrex tube containing a set of 50 stainless steel rings connected in series with 1 MΩ resistors

between the rings. The rings had an ID of 1.4 cm through which the flow passed. The chemical ionization reaction between the reagent ion and H_2SO_4 occurred in this region. A voltage was applied to the rings to enhance the ion flow. At the downstream end of the drift tube, the majority of the flow was diverted to a mechanical pump while a small portion of the flow was diverted through a pinhole into the MS.

The uptake coefficient (γ) is defined as the ratio of the molecules removed from the gas-phase to the total gas-surface collisions. The uptake process can be either reversible or irreversible. In some survey experiments, the movable injector was withdrawn to expose H_2SO_4 vapor to the soot film, and then pushed back to the original position. Changes in the H_2SO_4 signal intensity with the injector position clearly indicated that uptake of H_2SO_4 on soot was irreversible on the time scale of our experiments. The uptake coefficient or reaction probability (γ) was determined by observing the loss of sulfuric acid on the soot surface when the H_2SO_4 vapor was exposed to the soot film, and was calculated from the measured first-order rate constant (k) corresponding to the signal loss [*Keyser et al.*, 1991; *Zhang et al.*, 1994a; *Zhang et al.*, 1994b],

$$\gamma = 2rk / (\omega + rk)$$

where r is the radius of the flow tube and ω is the mean thermal speed. The uptake coefficient was determined using the geometric surface area of the soot-coated glass tube. To account for the H_2SO_4 radial gradients in the flow tube in the presence of a large reactant wall loss, the observed first-order loss rate constants (k_{obs}) were corrected for gas-phase diffusion with the method suggested by *Brown* [1978]. The H_2SO_4 gas-

phase diffusion coefficient in N_2 in the Brown calculations was adopted to be 69.1 Torr cm^2 s^{-1} at 298 K, an average of two literature values [*Poschl et al.*, 1998; *Hanson and Eisele,* 2000]. The corrections for gas-phase diffusion were 20-40% for small γ values ($\gamma < 0.01$) and as large as a factor of 1.7 for a γ value of 0.03. The γ value was investigated for fresh soot as well as soot that had been exposed to H_2SO_4 over an extended time period (about 20 minutes).

2.2.2. Characterization of H_2SO_4-Soot Interaction with FTIR. A schematic diagram of the experimental apparatus for soot generation, H_2SO_4 uptake, and characterization with FTIR is illustrated in Figure 2-2. Soot particles were produced by a gas or liquid burner, and sampled using a device similar to that described by *Kasper et al.* [1997]. A stainless steel tube (3/8" o.d.) was horizontally mounted with a 1 mm orifice drilled at the bottom. A filtered N_2 flow was used as a carrier gas to dilute the soot particles at a flow rate of 650 sccm. The soot-laden flow was subsequently introduced into a diffusion drier containing anhydrous $CaSO_4$ to reduce the relative humidity of the flow to below 5%. To coat soot with H_2SO_4, the dry soot particle flow was entrained into a 50cm long, 3cm i.d. Pyrex reservoir containing 96% H_2SO_4. Alternatively, in some experiments the soot particles bypassed the H_2SO_4 reservoir to obtain data without H_2SO_4 coating (i.e., fresh soot).

The IR spectra of the soot-H_2SO_4 particles were measured with a Fourier transform infrared spectrometer (FTIR, Nicolet Magna 560) equipped with an MCT detector in order to analyze the aerosol chemical composition. The aerosols were

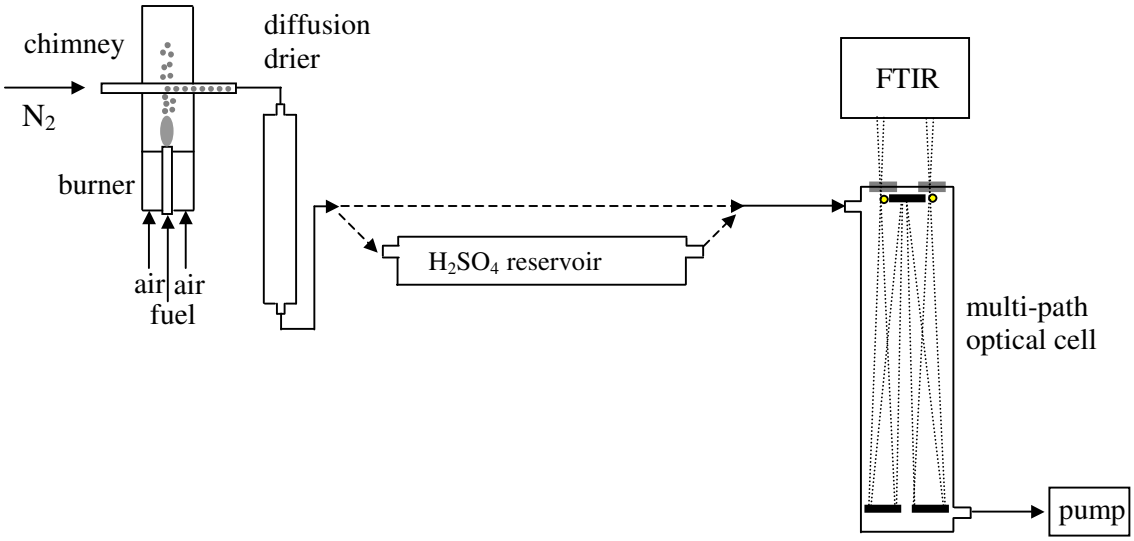

Figure 2-2. Schematic diagram of the experimental apparatus for soot generation, H_2SO_4 uptake and characterization using FTIR.

sampled *in situ* in a variable path-length long-path optical cell with two KCl windows (Infrared Analysis, Model 107-V). Spectra were recorded by averaging 24 scans in the typical wavenumber range from 4000 to 750 cm^{-1}. All IR spectra were measured at 4 cm^{-1} resolution.

2.3. Results and Discussions

2.3.1. Uptake Coefficient of Sulfuric Acid on Soot. Figure 2-3(a) shows a typical experiment illustrating that uptake of H_2SO_4 on soot is irreversible. The experiment was conducted at 1.6 Torr. A steady-state flow of H_2SO_4 in N_2 was first established through the movable injector pushed past the soot film. At about 85 s, the injector was quickly withdrawn to expose a 7 cm length of the soot film to H_2SO_4 vapor while monitoring the HSO_4^- signal in the mass spectrometer. A sharp decrease in the signal intensity was observed upon exposing H_2SO_4 to soot. No recovery in the H_2SO_4 signal was observed during the exposure. At about 230 s, the injector was moved downstream (*i.e*. the soot film was no longer exposed to H_2SO_4) and the HSO_4^- signal returned to its original level. This type of measurements clearly suggested an irreversible uptake of H_2SO_4 vapor on the soot surface under our experimental conditions.

The uptake coefficient measurements were conducted by observing the decay of the HSO_4^- (m/e = 97) signal as a function of the injector position as the injector was successively pulled upstream over the soot film. The HSO_4^- signal decay was found to be exponential according to the equation

$$I_t = I_0 \exp(-k_{obs}\, t)$$

where I_0 represents the initial HSO_4^- signal without uptake on soot, I_t is the signal at a

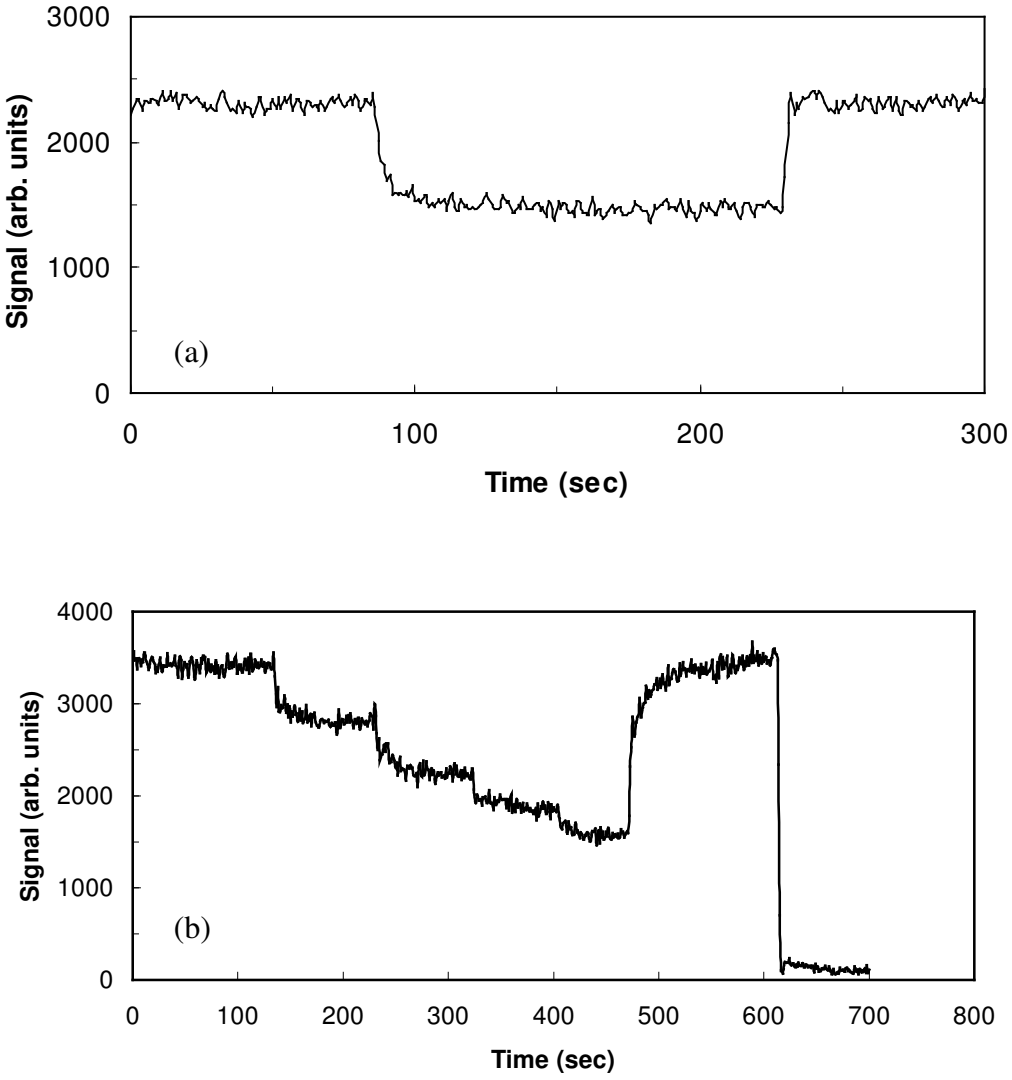

Figure 2-3. Time evolutions of the HSO_4^- (m/e = 97) signal. In (a) the injector was withdrawn to expose a 7 cm length of methane soot film to the H_2SO_4 vapor, and then returned to its original position. Experimental conditions: P_{total} = 1.55 Torr, U = 1515 cm s^{-1}, and T = 298 K. In (b) the injector was successively withdrawn for a total of 12 cm length over kerosene soot. Experimental conditions: P_{total} = 1.5 Torr, U = 2149 cm s^{-1}, and T = 298K.

given reaction time (or corresponding to a given injector position), and k_{obs} is the observed first-order loss rate constant.

Figure 2-3(b) illustrates a typical HSO_4^- signal decay on kerosene soot at various injector positions. The experiment was conducted at P_{total} = 1.5 Torr, U = 2149 cm s^{-1}, and T = 298K. The injector was successively withdrawn for a 3-cm distance over the soot surface between 130 and 470 s. At 470 s, the injector was pushed downstream to the original position and a full recovery of the signal was observed. At the end of the experimental run, the N_2 carrier gas bypassed the H_2SO_4 bubbler to obtain a background signal.

The first-order decay of the HSO_4^- signal was plotted against the reaction distance for each uptake experiment. Figure 2-4 shows typical HSO_4^- signal decays on kerosene soot as a function of injector position. The experiments were conducted at P_{total} = 1.4 Torr and U = 1864 cm s^{-1}. The filled circles represent data measured on fresh soot, while the open circles correspond to a measurement on soot after 20-min exposure to H_2SO_4. Both decays followed first-order kinetics. Linear regression analysis of each data set was performed to obtain the observed first-order rate constant k_{obs}. The loss of H_2SO_4 on fresh soot was found to be slightly higher than that on soot that had been exposed to H_2SO_4 for about 20 min. Accordingly, the γ value decreased slightly from 0.028 for fresh soot to 0.022 for the H_2SO_4 exposed soot. Similar behaviors were observed for H_2SO_4 uptake on all three types of soot (i.e., methane, hexane, and kerosene) over the pressure range of 1.3-1.7 Torr.

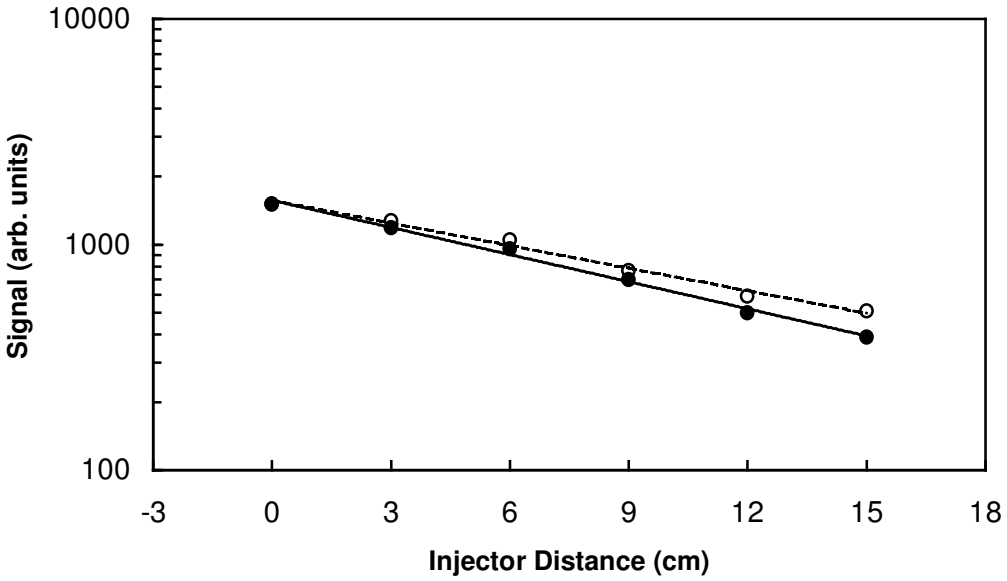

Figure 2-4. HSO_4^- (m/e = 97) signal as a function of injector position. Experimental conditions: P_{total} = 1.4 Torr, U = 1864 cm s^{-1}, and T = 298K. The filled circles and solid line represent the measurement on fresh soot; the open circles and dashed line represent the measurement on soot after about a 20 min exposure to H_2SO_4.

Significant deactivation of soot surfaces by chemical adsorption was previously reported for the uptake of NO_2 [*Longfellow et al.*, 1999], N_2O_5, and O_3 [*Longfellow et al.*, 2000]. In contrast to the previous studies, our measured decrease of γ was relatively minor for the H_2SO_4 uptake, usually within 20% for a ~20-min exposure time. Using an estimated average H_2SO_4 partial pressure of 5×10^{-8} Torr in the flow tube under our experimental conditions, the amount of H_2SO_4 taken up by ~78 cm^2 (geometric surface area) of soot was approximately 1×10^{15} molecules. Thus the fractional soot surface coverage was roughly 3% for 20-min exposure assuming a monolayer deposition of H_2SO_4 molecules. During each experimental run, the soot surface coverage was less than 1%.

Previous studies postulated possible chemical mechanisms for the irreversible uptake of certain inorganic species on soot. For example, the soot surface was proposed to serve as a catalytic site for reactions such as $NO_2 + H_2O$, which did not cause soot deactivation in the atmosphere [*Longfellow et al.*, 1999]. In other cases, soot was suggested to be oxidized by the adsorbed species, leading to soot deactivation. *Choi and Leu* [1998] proposed a bimolecular HNO_3 decomposition mechanism on soot surfaces, resulting in formation of NO, NO_2 and H_2O, as well as soot oxidation. No reaction product was detected in the mass spectra during our experiments. In addition, the lack of significant sign for soot deactivation during the 20-min time period suggests that the irreversible loss of H_2SO_4 on soot may involve little chemical reaction. Rather, it is likely due to the sticky nature of H_2SO_4 and the porous structure of soot. If the uptake is a pure physical adsorption process, the γ value should eventually approach that for

H_2SO_4 on H_2SO_4 when the soot surface is fully covered by H_2SO_4, which is 0.65 [*Poschl et al.*, 1998]. The reason for the observed decrease of γ value in the short 20-min term is currently unclear. Uptake coefficient measurements of H_2SO_4 on soot performed in this study are summarized in Table 2-1, along with the experimental conditions and the R^2 value for each linear fit. Since the decrease in uptake coefficients due to soot deactivation was within the error bars of our reported γ values, we did not differentiate the uptake coefficients on fresh soot from those on soot after H_2SO_4 exposure. For experiments conducted on three types of soot, small differences in the uptake coefficients were observed. The measured γ value was 0.018 ± 0.007 for kerosene soot at a total pressure of 1 to 2 Torr and 298 K, while smaller γ values were determined for methane (0.012 ± 0.006) and hexane (0.0076 ± 0.0016) soot under the same experimental conditions. The uncertainty represents the scatter in the data at the one standard deviation level and is not an estimate of systematic errors. We estimated that systematic uncertainty in our measured rate constants was within $\pm$ 10%, considering the possible sources of error in the measurements (i.e., gas flows, temperature, detection signal, and pressure) and in the gas-phase diffusion corrections. The uncertainty, however, did not include that associated with the assumption using the geometric area of deposited soot, to be discussed below.

Table 2-1. Summary of Uptake Coefficient Measurements of H_2SO_4 on Soot.[a]

Soot Type	P_{total} (Torr)	U (cm/s)	R^2	γ
Methane	1.56	1515	0.987	0.010*
	1.56	1815	0.982	0.014*
	1.51	1971	0.979	0.020*
	1.51	1971	0.990	0.013
	1.51	1971	0.979	0.015
	1.51	1494	0.995	0.0053
	1.51	1494	0.992	0.0043
				Average[b] = 0.012 ± 0.006
Hexane	1.50	1342	0.993	0.0083*
	1.56	1394	0.994	0.0080*
	1.51	1748	0.989	0.011*
	1.51	1748	0.999	0.0054
	1.50	1715	0.978	0.0080*
	1.56	1720	0.997	0.0062*
	1.56	1720	0.996	0.0056
	1.56	2246	0.988	0.0079*
	1.54	2393	0.987	0.0084*
	1.54	2393	0.993	0.0068
				Average[b] = 0.0076 ± 0.0016
Kerosene	1.51	2149	0.997	0.017*
	1.51	2149	0.978	0.014
	1.51	2149	0.984	0.014
	1.54	2402	0.995	0.011
	1.30	1768	0.994	0.014*
	1.30	1768	0.991	0.0096
	1.71	2461	0.974	0.0097
	1.51	1951	0.974	0.011*
	1.51	1951	0.994	0.0088
	1.51	1946	0.976	0.010
	1.50	2010	0.991	0.030*
	1.40	1864	0.995	0.028*
	1.40	1864	0.989	0.022
	1.50	2005	0.994	0.027*
	1.60	2148	0.990	0.021*
	1.70	2307	0.998	0.015*
	1.50	2006	0.973	0.024*
	1.51	1971	0.966	0.027*
	1.51	1971	0.982	0.024
	1.51	1971	0.970	0.022
				Average[b] = 0.018 ± 0.007

[a] Values with an asterisk correspond to measurements on fresh soot, whereas values without the asterisk correspond to measurements on soot after about 20 min exposure to H_2SO_4.
[b] Averages are given with the range of one standard deviation of the mean.

The uptake of other inorganic species on soot was found to vary considerably for different soot types. For example, in a recent study of the interaction of water vapor with soot, initial uptake coefficients of H_2O on toluene, acetylene, and diesel soot were determined, while no measurable interaction between H_2O and decane soot was observed at ambient temperature [*Alcala-Jornod and Rossi*, 2004]. Similarly, the uptake coefficient of HNO_3 was found to vary considerably on FW2 carbon black, graphite, hexane and kerosene soot [*Choi and Leu*, 1998]. In a study of NO_2 uptake on methane, hexane, propane, and kerosene soot, the uptake coefficient was found to vary within an order of magnitude for the different soot types [*Longfellow et al.*, 1999].

Our calculated γ values were based on the geometric surface area assumption, i.e., taking the surface area coated by soot in the flow tube as the soot surface area for reaction. In reality the deposited soot film might be highly porous and exhibit a large internal surface area. Using the Brunauer, Emmett, and Teller (BET) surface area of 25 $m^2\ g^{-1}$ for methane soot [*Tesner and Shurupov*, 1995], 91 $m^2\ g^{-1}$ for kerosene soot and 46 $m^2\ g^{-1}$ for hexane soot [*Choi and Leu*, 1998], γ would be predicted to be approximately a factor of 5-18 less than that assuming a geometric surface area for a typical amount of 2 mg soot in our experiments, considering the difference in surface area. Our reported γ values would represent the upper limit if the BET surface needs to be taken into account. To investigate the dependence of the uptake coefficient on internal surface areas, we performed additional experiments to measure γ for various total masses of the deposited soot. In all experiments, no apparent dependence of the measured γ on soot mass was observed in the mass range of 1-10 mg. Similar mass independence of γ was found for

NO_2 [*Longfellow et al.*, 1999] and HNO_3 uptake on kerosene soot [*Choi and Leu*, 1998] and HNO_3 uptake on NaCl and KBr [*Fenter et al.*, 1996]. There are several possible explanations to account for the lack of the mass dependence of the measured γ. The soot films had many layers of packing and the H_2SO_4 vapor likely only sampled a limited portion of micropores. It was also plausible that the sticky nature of H_2SO_4 made diffusion into internal layers difficult and only the upper layers were reached by H_2SO_4 molecules, as proposed for HNO_3 uptake on NaCl and KBr [*Fenter et al.*, 1996] and HNO_3 uptake on kerosene soot [*Choi and Leu*, 1998]. Hence H_2SO_4 diffusion into the internal surface would be much slower than predicted by simplified diffusion models [*Choi and Leu*, 1998]. The effect of internal surface areas of soot on the uptake coefficient of H_2SO_4 requires further experimental and theoretical studies.

Our experiments were conducted under low relative humidity (RH < 1%). We were unable to measure the uptake coefficient at high RH since binary homogeneous nucleation of H_2SO_4 and H_2O occurred [*Zhang et al.*, 2004] and complicated the measurements. A previous study investigating HNO_3 uptake on n-hexane soot found little dependence on RH for RH as high as 80% [*Aubin and Abbatt*, 2003]. Low surface density of water adsorption sites was suggested as a possible explanation. Our own measurements of hygroscopicity of methane, hexane and kerosene soot showed that those three soot types were hydrophobic (Chapter III). In the previous study of the mass accommodation coefficient of H_2SO_4 vapor on aqueous H_2SO_4, it was also concluded that the observed wall loss coefficient of H_2SO_4 vapor was independent of the gas-phase H_2O concentration in the range of $(5\times10^{12}$ - $3\times10^{16})$ molecule cm^{-3} which was correlated

with RH [*Poschl et al.*, 1998]. According to these results, we expect the uptake coefficient of H_2SO_4 on soot to be independent of relative humidity.

All uptake experiments in this work were conducted at 298 ± 2 K. In a previous study of the gas-phase adsorption of HNO_3 on *n*-hexane soot, the uptake was found to increase with decreasing temperature between 228 K and 298 K, with a negative enthalpy of adsorption [*Aubin and Abbatt*, 2003]. Similarly, the adsorption of H_2O vapor on soot was found to be exothermic in the range of 190 K to 300 K [*Alcala-Jornod and Rossi*, 2004]. Nevertheless, recent studies suggested that the reactive uptake coefficients for NO_2 and O_3 on various hydrocarbon flame soot were independent on temperature over the range of 240-350 K [*Lelievre et al.*, 2004a; *Lelievre et al.*, 2004b]. The uptake of H_2SO_4 on soot should likely follow the exothermic mechanism similar to HNO_3 and H_2O, due to its non-reactive nature. The temperature-dependent behavior of the uptake coefficient of H_2SO_4 on soot is under further investigation, which will elucidate the thermodynamics of such processes.

2.3.2. Characterization of the Interaction of H_2SO_4 with Soot Using FTIR. In order to characterize the chemical composition of soot particles with H_2SO_4 adsorption and to further investigate the uptake mechanism of H_2SO_4 on soot, we performed FTIR spectroscopic measurements for soot particles with and without H_2SO_4 coating. Figure 2-5 shows the FTIR spectra of methane soot without (spectrum a) and with (spectrum b) H_2SO_4 exposure. The pressure inside the multi-path cell was kept at 1 atm for all FT-IR experiments due to the relatively low sensitivity of the technique. The absorption features of soot were attributed to the carbon skeleton, such as –C≡C-H (2180, 2120 cm^-

^{1}) and aromatic -C-H (3016 cm^{-1}), and –O-H group (3320, 3270 cm^{-1}). In a previous FTIR study using filter-deposited soot samples, much broader bands at 800-1600 cm^{-1}, 2800-3000 cm^{-1}, and 3200-3700 cm^{-1} were observed compared with the IR peaks from this study [*Kirchner et al.*, 2000]. This is likely due to the large absorption caused by deposited soot samples compared with the suspended soot aerosols in this work, although the authors also attributed the broader bands to possible reaction products during the soot generation processes. In two early spectroscopic studies of hexane soot, absorption bands at 1260 cm^{-1}, 1440 cm^{-1}, 1590 cm^{-1}, 1700-1800 cm^{-1}, and 3040 cm^{-1} were identified for carbon skeleton, oxygenated groups and –OH [*Akhter et al.*, 1985a; *Akhter et al.*, 1985b]. We did not observe significant peaks in the region of 1400-2000cm^{-1}, possibly because they were not adequately resolved in the IR spectrum for small H_2SO_4-containing soot aerosols.

Distinct S-O features were observed after the soot particles were exposed to H_2SO_4. Several absorption peaks at 1260 cm^{-1}, 1100 cm^{-1}, and 810 cm^{-1} appeared for the sample of H_2SO_4 coated aerosols. Those IR bands are close to those previously reported for liquid sulfuric acid, characteristic of the band locations of SO_4^{2-} and HSO_4^{-} [*Zhang et al.*, 1993a; *Middlebrook et al.*, 1993]. The sulfate bandwidths at half height for the H_2SO_4 coated soot aerosols are typically in the range of 15-25 cm^{-1}, much smaller than those collected using bulk liquid solutions which are generally 100-200 cm^{-1} [*Zhang et al.*, 1993a; *Middlebrook et al.*, 1993]. The narrow absorption bands are typical for S-O characteristics in the aerosol phase, as were also observed for $(NH_4)_2SO_4$ aerosols where the widths for SO_4^{2-} bands were in the range of 14-44 cm^{-1} [*Weis and Ewing*, 1996]. As

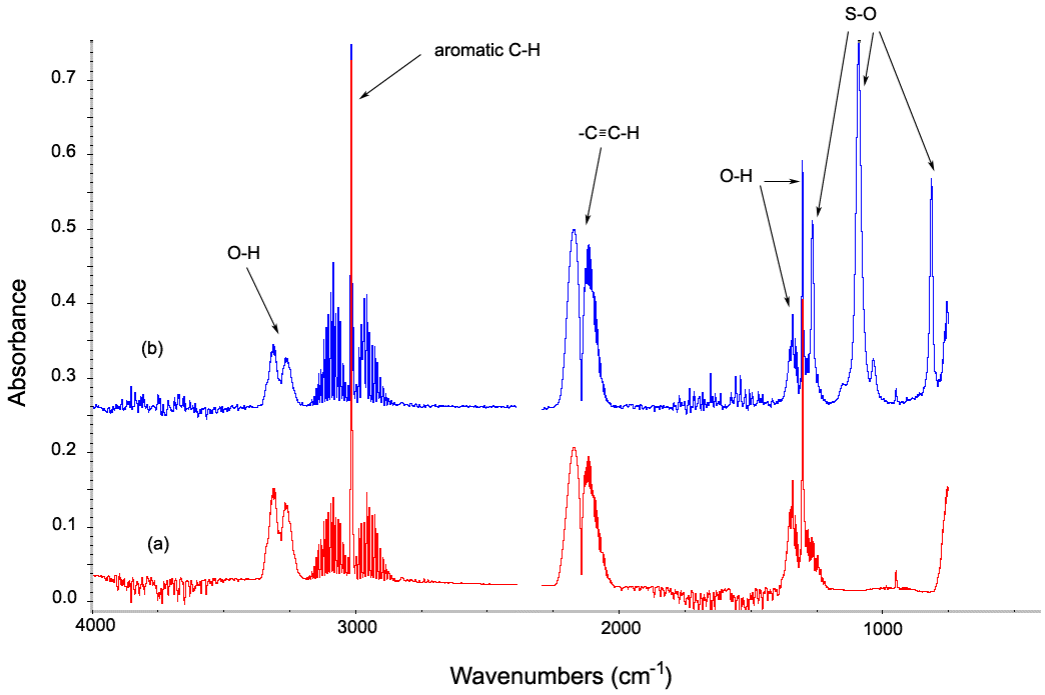

Figure 2-5. IR spectra of (a) fresh methane soot aerosols and (b) methane soot-H_2SO_4 mixed aerosols measured in the multi-path optical cell. Spectra are baseline corrected, intensity normalized, and shifted for clarity. The blank between 2300 and 2400 cm^{-1} was originally a peak due to CO_2 from the combustion and was removed from the spectra.

discussed above, our experiments were performed under low RH conditions, and hence homogeneous nucleation of H_2SO_4/H_2O to form external mixture of soot and sulfate aerosols was precluded.

Two other observations were made on the basis of analysis of the IR spectra. First, the absorption bands of soot particles attributing to the carbon skeleton, such as the –C≡C-H, aromatic, and –O-H groups, did not change appreciably after exposure to H_2SO_4 vapor. Also, if chemical reactions did occur on the soot surfaces, the IR spectrum of soot-H_2SO_4 mixed aerosols might exhibit more oxygenated functionalities, such as –C-O and –C=O, as a result of oxidation of the soot surface. Such oxygenated functional groups were not evident in the IR spectra of the H_2SO_4 coated soot aerosols. Hence the irreversible uptake of H_2SO_4 on soot observed in the flow reactor experiments is not likely due to chemical reactions.

The results of H_2SO_4 uptake on soot particles are crucial to understand how the soot-H_2SO_4 aerosols influence the atmospheric radiative balance, heterogeneous chemistry, and their CCN forming potential. The present study reveals efficient uptake of H_2SO_4 for three types of soot, which are relatively fast compared with the uptake of other inorganic atmospheric species (such as HNO_3 or NO_2) on soot. This suggests that the adsorption on soot of H_2SO_4 likely represents an important way to convert hydrophobic soot into CCN, considering the large abundance of soot and H_2SO_4 in the atmosphere from combustion, industrial sources, automobile and aircraft emissions.

2.4. Summary

We have reported the first measurements of uptake coefficients of H_2SO_4 on three types of soot at the temperature of 298 K and in the pressure range of 1 to 2 Torr. H_2SO_4 loss on soot was found to be irreversible. A slight decrease in the uptake coefficient was observed with extended exposure of soot to H_2SO_4. Additional experiments using Fourier transform infrared spectrometer (FTIR) techniques confirmed the interaction of H_2SO_4 with soot. The results imply that the heterogeneous reactions between soot and sulfuric acid proceed efficiently and that the activation of soot by H_2SO_4 represents an important way to convert hydrophobic soot into CCN.

CHAPTER III

HYGROSCOPIC GROWTH OF SOOT-CONTAINING AEROSOLS

3.1. Introduction

Freshly emitted soot in the atmosphere is subjected to several aging processes, such as adsorption and condensation of gaseous species on soot surfaces [*Zhang and Zhang*, 2005], coagulation of soot with other pre-existing aerosol constituents [*Kotzick and Niessner*, 1999], and oxidation of soot by various atmospheric species [e.g., *Choi and Leu*, 1998]. Internally mixed soot particles are also produced from burning fuels with sulfur-containing additives. The hygroscopicity of soot is altered during the aging processes, which has an important influence on its residence time, optical properties and cloud-forming potential. Previous studies have indicated that jet and diesel engine combustion soot particles are hygroscopic [*Hagen et al.*, 1992; *Pitchford et al.*, 1991; *Gysel et al.*, 2003], commonly attributable to sulfuric acid adsorption on soot surfaces that enhance water uptake below saturation [*Wyslouzil et al.*, 1994]. Other field and laboratory investigations have revealed that aircraft engine soot is a primary contributor to contrail nuclei due to the impurities containing soluble sulfates and organics [*Karcher et al.*, 1996; *Popovicheva et al.*, 2004]. In addition, the activation of soot particles as cloud condensation nuclei (CCN) is found to be enhanced by the uptake of water-soluble inorganic species such as H_2SO_4 and HNO_3 [*Schumann et al.*, 1996; *Hallett et al.*, 1989]. Previous laboratory experiments have also confirmed that soot aerosols are incorporated into existing cloud droplets when they are internally mixed with water soluble components, leading to wet deposition [*Lamel and Novakov*, 1995]. There likely exist

multiple impacts of fresh or aged soot on the global climate. They can directly absorb and scatter solar radiation, hence affecting the global radiative budget [*Jacobson*, 2001]. In addition, soot particles also act as CCN that changes the cloud formation processes and subsequently impacts the cloud albedo [*Ackerman et al*., 2000; *Rosenfeld D.*, 2000; *Breon et al., 2002; Twomey et al*., 1984].

The hygroscopicity of an aerosol likely depends on several factors, including the size, chemical composition, morphology, and wetability (contact angle) of the particle. Freshly generated soot particles exist in the form of aggregates composed of hydrophobic primary particles. The irregular geometry and complex microstructure of the soot aggregate surfaces provide possible active sites for water deposition. Measurements of the water/ice contact angle on surfaces of aircraft combustion soot and kerosene soot showed a range from 60° to 80°, suggesting that the adsorption of water on the insoluble surface was facilitated by capillary condensation on surface active sites [*Persiantseva et al.*, 2004]. An analysis of the primary contrail particles from the aircraft engine indicated that soot from zero sulfur content fuel could still take up water and act as contrail nuclei [*Karcher et al.*, 1996]. A recent laboratory study revealed that sulfur-free combustor soot acquired a substantial fraction of a water monolayer even in the young plume due to the specific microporous structure and surface heterogeneity [*Popovitcheva et al.*, 2001]. Laboratory-generated kerosene soot was found to exhibit a high potential for water freezing in another study [*Ferry et al.*, 2002]. In contrast, a recent light reflectometry investigation did not detect water uptake (activation) on

laboratory-generated fresh methane and hexane soot even at 115% relative humidity (RH) [*Zuberi et al.*, 2005].

Many of the previous studies on water uptake and hygroscopicity of combustion soot examined soot produced from fuels with various sulfur contents. Aging of freshly emitted soot by adsorption of trace gaseous species in the atmosphere represents another important mechanism to produce internally mixed soot particles. A chamber study during the European AIDA Soot Aerosol Campaign revealed that secondary organic aerosol (SOA) coating from α-pinene ozonolysis increased the hygroscopic growth factors of soot to values closely below the growth factors measured for pure SOA material [*Saathoff et al.*, 2003a]. However, the impact of the other important chemical coatings, especially sulfuric acid, on the hygroscopicity of aged soot remains uncertain. There lacks quantitative information on the variation of the hygroscopicity of soot when internally mixed with sulfuric acid. In this chapter, we report an experimental study on the hygroscopicity of both freshly generated flame soot and soot with a sulfuric acid coating, using a combustion-aerosol chamber in conjunction with tandem differential mobility analyzer (TDMA) detection. In addition, the morphology of both soot types is examined by transmission electron microscopy (TEM) to evaluate the microstructure and mixing state of soot. The results improve our understanding of the impact of soot coating on its hygroscopicity and CCN forming potential.

3.2. Experimental Section

A schematic of the experimental setup for soot generation, mixing, and hygroscopicity measurements is shown in Figure 3-1. Soot particles were generated by

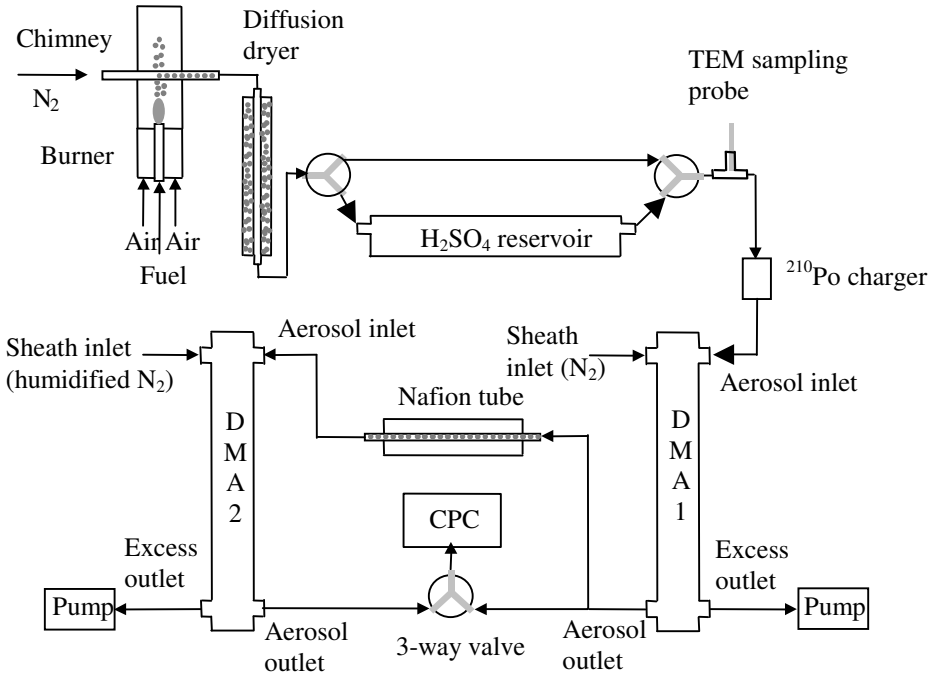

Figure 3-1. Schematic diagram of the experimental apparatus for soot-containing aerosol generation and hygroscopicity measurements.

burning three types of fuels, methane, propane and kerosene, in the laboratory. A Santoro-type laminar diffusion burner was used to produce soot with gaseous fuels [*Santoro et al.*, 1983]. The burner consisted of two concentric tubes, with the fuel flowing through a 7 mm i.d. inner tube and the air through a 66 mm i.d. outer tube. Typical flow rates for generating methane and propane soot are summarized in Table 3-1. The flame height was generally 4-5 cm. Kerosene soot was produced in a commercial kerosene lamp. The soot sampling system was similar to that described by *Kasper et al.* [1997], consisting of a horizontally mounted stainless steel tube of 7 mm i.d. with a 1 mm orifice drilled at its bottom. Soot particles were collected through the orifice and diluted by a 200 cm^3 min^{-1} N_2 carrier gas flow. A glass chimney was placed on the top of the burner to shield the flame from ambient disturbance. The soot-laden flow was subsequently introduced into a diffusion drier to reduce the RH to < 5%. Soot particles were then either exposed to sulfuric acid vapor in a 50 cm long, 3 cm i.d. reservoir containing 96 wt % H_2SO_4 at room temperature, or entrained directly into the TDMA detection system as fresh soot.

The size, morphology, and mixing state of soot were examined using a JEOL 2010 transmission electron microscope (TEM), which was operated at an accelerating voltage of 200 kV. Samples of the soot-containing aerosols were collected on Cu TEM grids (200 mesh with amorphous carbon film) mounted on the tip of stainless steel probe which was inserted downstream of the H_2SO_4 reservoir. TEM images of the aerosol samples were obtained at magnifications ranging from 50,000 to 150,000 times.

Table 3-1: Representative Flow Rates for Generation of Methane and Propane Flame and for DMA Sampling.

Diffusion Burner	
Methane flame	
Methane	150 cm^3 min^{-1}
Air	3.0 L min^{-1}
Propane flame	
Propane	50 cm^3 min^{-1}
Air	1.5 L min^{-1}
DMA	
Aerosol inlet	650 cm^3 min^{-1}
Sheath (N_2) inlet	6.5 L min^{-1}
Aerosol outlet	650 cm^3 min^{-1}
Excess outlet	6.5 L min^{-1}

Additional high-resolution images were taken at a 400,000 × magnification for analyzing the nano-structure of soot primary particles.

Measurements of aerosol size distributions and hygroscopic growth were conducted using a tandem differential mobility analyzer (TDMA) system illustrated in Figure 3-1. It consisted of two differential mobility analyzers (DMA, TSI 3081) and a condensation particle counter (CPC, TSI 3760A). A similar TDMA system was employed previously to study the hygroscopicity of ambient aerosols [*Gasparini et al.*, 2004]. Experiments were conducted by operating in a single DMA or TDMA mode with the control of a three-way valve. Typical flow rates in each DMA are also summarized in Table 1. During an experiment, the polydisperse soot-containing aerosols were initially brought to charge equilibrium by a Po-210 bipolar diffusion charger prior to entering the first DMA. In the DMA operation mode, the particle size was varied over time by scanning the voltage applied to the DMA while the particles were counted continuously. The size distribution was determined by combining the particle size and number concentration and accounting for the instrument response. In the TDMA mode, the dry aerosol stream was reduced to a monodisperse flow by applying a fixed voltage to the first DMA. This monodisperse flow was then exposed to an elevated-RH environment in a Nafion tube (Perma Pure Inc.), where the RH was accurately controlled between approximately 20% and 80% by a valve using a software-based algorithm. The hygroscopic growth distribution was determined by simultaneously scanning the voltage on the second DMA and counting the particles. The hygroscopic growth was expressed in terms of a ratio of D_p to D_o, where D_p was the hydrated particle diameter and D_o the

dry particle diameter. Humidified N_2 was used for the sheath flow of the second DMA to prevent possible evaporation of the soot particles. Two RH probes were mounted before and after the second DMA to ensure a RH within 2% in the sheath flow and the Nafion tube. The size-resolved hygroscopic growth of both fresh and H_2SO_4-treated soot was studied as a function of RH and particle size.

In addition to the hygroscopic growth measurements at subsaturated conditions, we performed Köhler calculations to estimate the critical supersaturation of aged soot of various sizes. CCN measurements were also conducted for the soot-containing particles at various supersaturations using a CCN counter (Droplet Measurement Technologies) in conjunction to a TDMA system. The size distributions for the dry particles (condensation nuclei, CN) and particles that are activated (CCN) are measured at each given supersaturation. The activation size can hence be deduced from the ratio of the CCN/CN size distributions

3.3. Results and Discussions

3.3.1. Morphology. The size and morphology of both fresh and H_2SO_4-exposed soot generated from the three types of fuels were studied by TEM. Figure 3-2 shows the TEM images of the soot-containing aerosols. A previous TEM study revealed that the morphology of flame soot was closely related to the global equivalence ratio (the fuel-air ratio divided by the fuel-air ratio under stoichiometric conditions) [*Widmann et al.*, 2003]. The spherical primary particles were clearly noticeable under stoichiometric conditions. When the equivalence ratio was increased, the soot aggregates generated at under-ventilated conditions had the appearance of "fused" primary particles. The authors

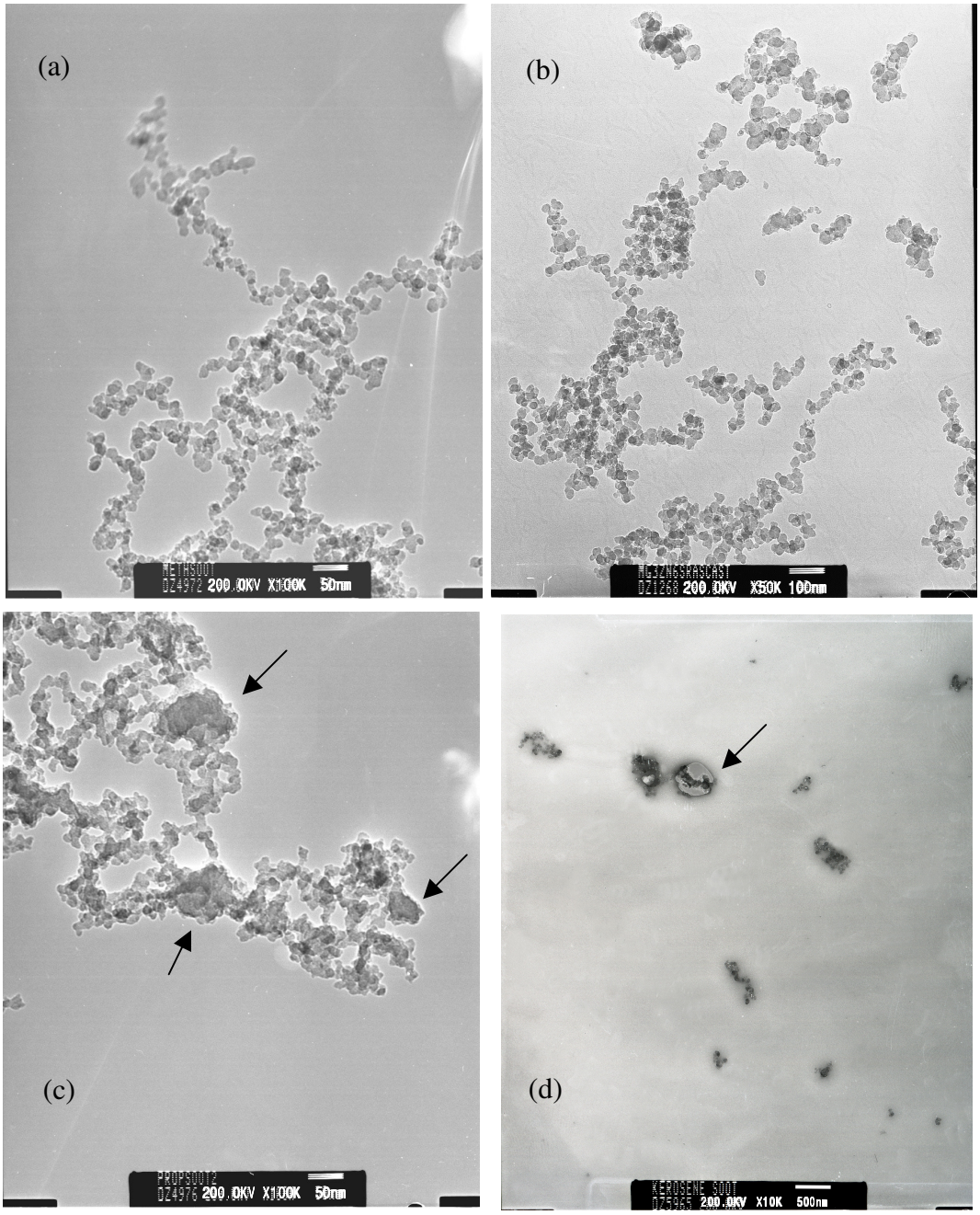

Figure 3-2. TEM images of various soot-containing aerosols. (a) air-rich fresh methane soot, (b) air-rich fresh propane soot, (c) fuel-rich propane soot after exposure to H_2SO_4 vapor, (d) kerosene soot after exposure to H_2SO_4 vapor.

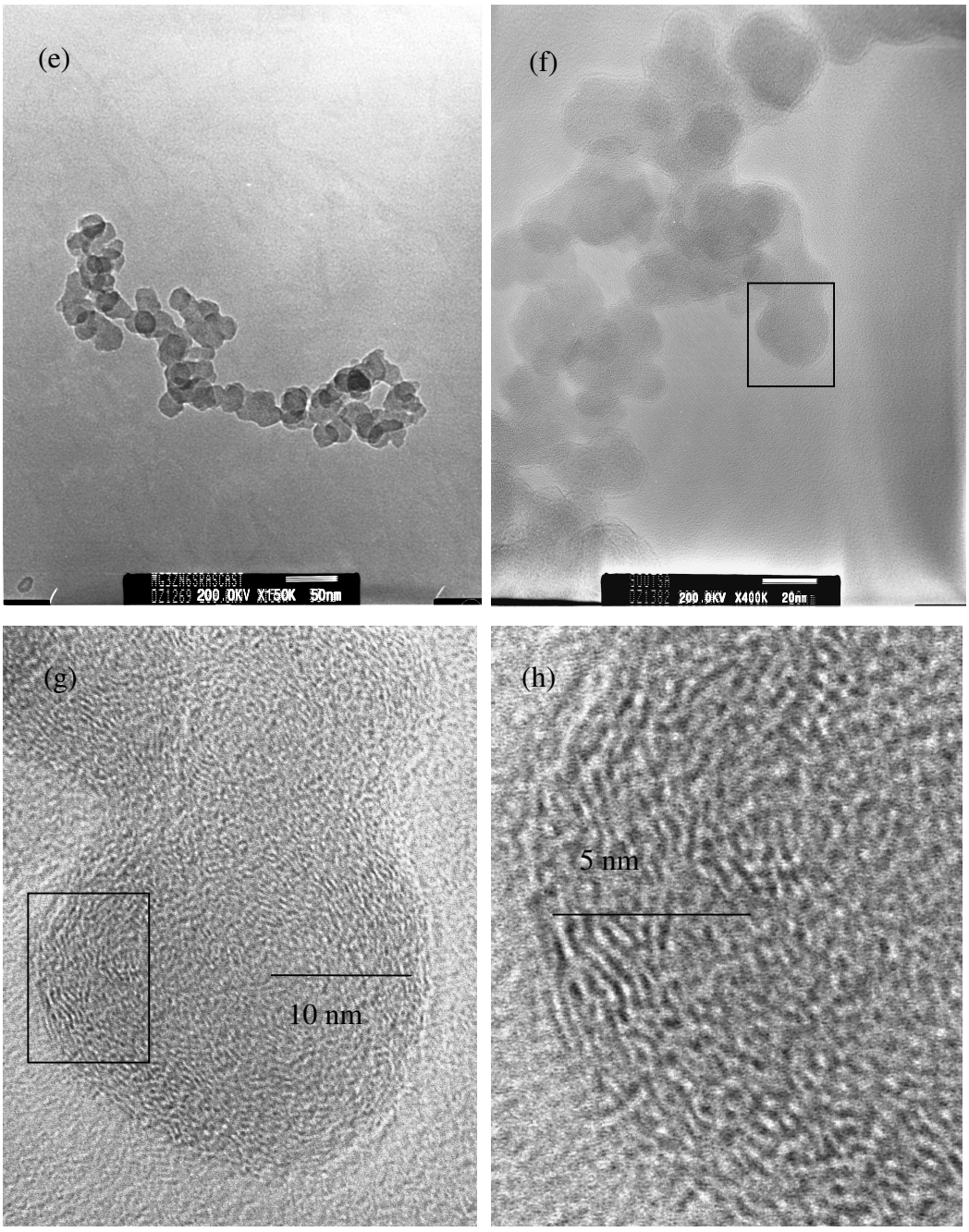

Figure 3-2. (cont'd) (e) typical chain structure of a kerosene soot aggregate, (f) a high resolution image of soot aggregate, (g) an enlarged image of the selected rectangular area from (f), and an enlarged image of the selected rectangular area from (g). Arrows indicate likely internal mixtures of soot with H_2SO_4.

attributed the differences to enhanced ratio of organic to elemental carbon in the fuel-rich soot particles due to incomplete combustion. In our experiments, soot was typically generated under air-rich conditions with the equivalence ratios of 0.5 and 0.8 for methane and propane soot, respectively. Figures 3-2 (a) and (b) illustrate the structures of fresh methane and propane soot: the soot particles are predominantly chain-like aggregates and the spherical primary particles are clearly identifiable. In the case depicted by Figure 3-2 (c) where propane soot was produced with an equivalence ratio of 1.25, the primary particles appear more blended with less clear boundaries.

Previous TEM studies also identified internal mixtures of soot with ammonium sulfate from both field and laboratory samples [*Posfai et al.*, 1999; *Wentzel et al.*, 2003]. Soot appeared to be on the surface of an ammonium sulfate particle in the laboratory-generated internal mixtures, while inclusions of soot within ammonium sulfate were found in atmospheric samples due to the deliquescence of ammonium sulfate under ambient RH conditions. In the present study, the internal mixtures of soot with H_2SO_4 were observed by TEM for soot samples collected after exposure to the H_2SO_4 vapor. Although sulfuric acid on the TEM grid was subjected to evaporation under vacuum conditions in the TEM chamber, residue of sulfuric acid was still observable, as marked by the arrows in Figures 3-2 (c) and (d) for propane and kerosene soot samples, respectively. The internal mixture appeared to be composed of one or more soot aggregates with sulfuric acid inclusion. No individual sulfuric acid aerosol was identified in all soot-H_2SO_4 mixed samples.

The three types of flame soot studied in this work exhibited the similar chain aggregate structure as enlarged in Figure 3-2 (e). The sizes of the soot aggregates ranged from 50 to 300 nm. Note that the size selected by a DMA represented the electron mobility diameter, which was a geometric effective diameter and was hence different from the real size of a soot chain aggregate observed in TEM images. The primary particle diameters of the three types of soot were measured where the primary particles were clearly identified in the aggregates. The primary particle sizes of kerosene soot were in the range of 21-30 nm, comparable to those of combustor soot from diesel and gas turbine engines [*Wentzel et al.*, 2003; *Popovitcheva et al.*, 2000], while methane and propane soot possessed smaller primary particles, with the diameters ranging from 13 to 17 nm for methane soot and 15-20 nm for propane soot. The microstructure of primary soot particles was also studied by high-resolution imaging as illustrated in Figure 3-2 (f). As seen in the enlarged Figures 3-2 (g) and (h), the primary particles were composed of carbon layers concentrically arranged in an onion-shell structure. This implied that primary soot particles contained nanocrystalline graphite, similar to previous examinations of soot from atmospheric samples as well as diesel and aircraft engines [*Posfai et al.*, 1999; *Wentzel et al.*, 2003; *Popovitcheva et al.*, 2000], while primary particles were found to be amorphous for aircraft engine soot in another study [*Popovicheva et al.*, 2004].

3.3.2. Hygroscopicity Measurements. The overall particle size distributions of flame soot with and without exposure to H_2SO_4 vapor were obtained using DMA-1 and the CPC. Figure 3-3 shows the differential concentrations of propane soot under typical

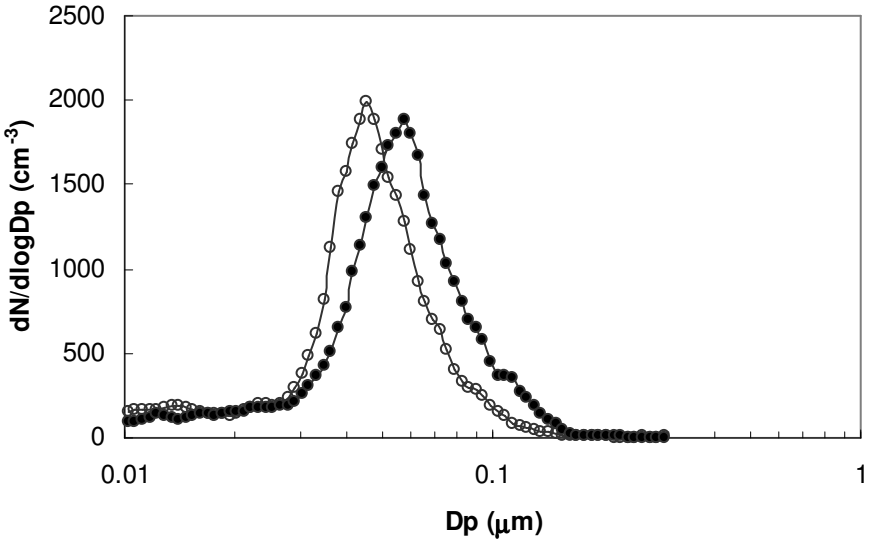

Figure 3-3. Size distributions of propane soot aerosols with (filled circles) and without (open circles) passing through the H_2SO_4 reservoir.

experimental flow conditions as a function of the particle mobility diameter. In this case, the particle size at the peak concentration shifted from 46 nm for fresh soot to 57 nm for soot with H_2SO_4 exposure, indicating an increase in the particle size because of H_2SO_4 coating. A previous investigation of the size distributions of premixed ethylene soot indicated that the mean particle size increased with both enhanced equivalence ratio and elevated flame height [*Maricq et al.*, 2003]. We also observed a dependence of the soot size distribution on the fuel/air ratio and height of flame. The present flow rates for fuels and air were chosen in order to produce a size distribution with the mean diameter between 40 and 70 nm so that a range of dry particle sizes could be selected for the hygroscopicity measurements within the DMA detection limit.

When soot particles passed through the H_2SO_4 reservoir, the resulting aerosol stream possibly contained both internally mixed soot-H_2SO_4 aerosols and external mixture of separate soot and H_2SO_4 aerosols. If the aerosols existed exclusively in an internal mixing state, exposure to H_2SO_4 vapor would cause an increase in the soot particle size but without a significant change in the number concentration, as was illustrated in Figure 3-3. If new H_2SO_4 particle were generated because of binary nucleation of H_2O-H_2SO_4 to form an external mixture, one would expect to observe a change in the particle concentration and possibly a bimodal distribution for soot after passing the H_2SO_4 reservoir. No apparent external mixing of the soot-H_2SO_4 aerosols was detected in all our measurements, because the extreme low RH of the soot flow prior to entering the H_2SO_4 container prohibited new H_2SO_4 particle formation. This was also confirmed by the TEM study where no distinct H_2SO_4 aerosol was observed.

The hygroscopic growth of both fresh and H_2SO_4-coated soot was investigated at various dry particle diameters between 30 and 100 nm and as a function of RH. For all dry particle sizes and all three soot types, the growth factor for fresh soot was found to be 1.00 ± 0.01 in the RH range of 20% to 80%, indicating no growth or shrinking within the detection sensitivity. Figure 3-4 shows an example of the hygroscopic growth distributions of fresh propane soot at 80% RH for the dry particles sizes of 30 nm, 50 nm and 70 nm. Although previous studies indicated that diesel engine and aircraft combustor soot from sulfur-free fuels could still take up water under subsaturated conditions and act as contrail nuclei [*Weingartner et al.*, 1997; *Karcher et al.*, 1996; *Popovitcheva et al.*, 2001], it is likely that soot emitted from combustion engine contains more organic carbon than flame soot generated in well-ventilated conditions in the present study, and is therefore more hygroscopic. In another hygroscopic study of carbon particles produced by spark discharges [*Weingartner et al.*, 1995], the particles were found to shrink to about 85% of the dry size at 90% RH. The authors attributed this behavior to the collapse of highly branched particles following the capillary condensation in small angle cavities of the aggregates. Although the flame soot in this study was also highly aggregated, no apparent restructuration was observed. It is plausible that the spark-generated soot exhibits different surface chemical composition and microstructure from the methane, propane and kerosene flame soot and capillary condensation of water is more likely to occur, leading to restructuration.

Considerable hygroscopic growth was observed for H_2SO_4-coated soot at RH > 60% with all selected dry particle sizes and all three types of fuels. Figure 3-5 indicates

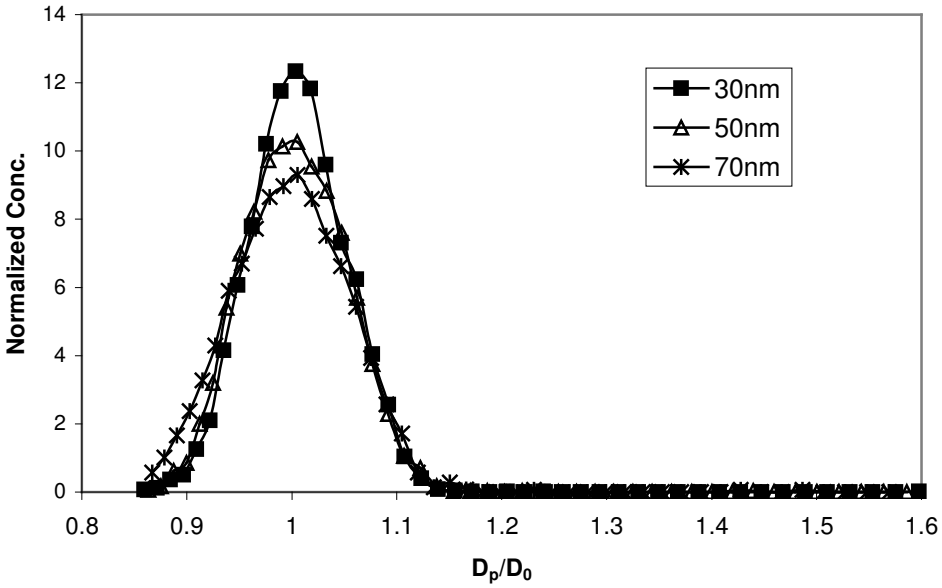

Figure 3-4. TDMA size distributions of fresh propane soot at 80% RH for various dry particles sizes. D_p/D_o represents the hygroscopic growth factor.

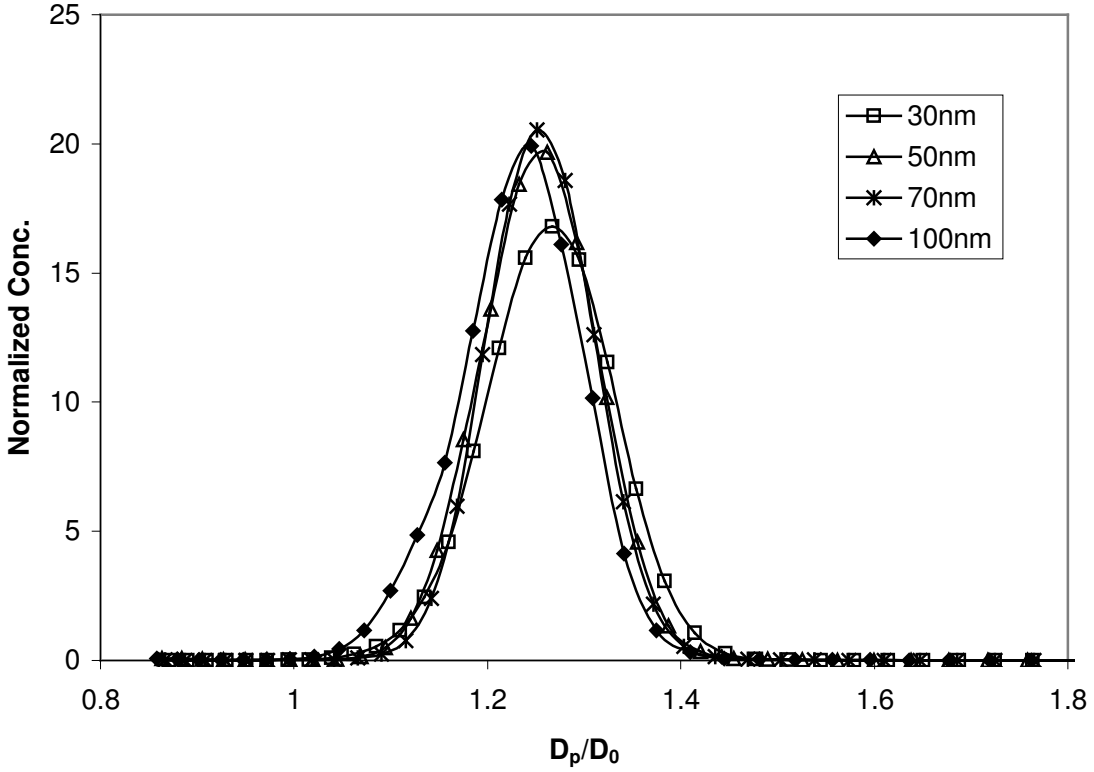

Figure 3-5. TDMA size distributions of H_2SO_4-coated propane soot at 65% RH for various dry particles sizes. D_p/D_o represents the hygroscopic growth factor.

the TDMA hygroscopic growth of H_2SO_4-coated propane soot at 65% RH for various dry particles sizes. The growth factors were between 1.24 and 1.26 for dry particle sizes of 30 nm, 50 nm, 70 nm and 100nm. A slight tendency of decreasing growth factor with increasing particle size was evident in Figure 3-5, but this size-dependent hygroscopic growth was within the uncertainty of our experiments. The amount of water adsorbed on the surface of H_2SO_4-coated soot aerosols is likely determined by both the volume fraction of the adsorbed H_2SO_4 and the particle size. Larger particles tend to condense more water according to the Kelvin effect, but this effect may be counteracted by less H_2SO_4 volume fraction in larger particles. In a recent hygroscopicity study of jet engine combustion particles, which were assumed to be soot coated with H_2SO_4, the hygroscopic growth factor was found to increase distinctively with decreasing dry particle size, suggesting a higher H_2SO_4 volume fraction in smaller particles [*Gysel et al.*, 2003]. The authors attributed the size dependence of H_2SO_4 fraction to the relatively larger mass accommodation of smaller particles leading to more condensation of gaseous sulfuric acid. It is likely, though, the hygroscopic growth of flame soot with extreme irregularity and complex microstructure may be distinct from that of the more compact and less chain-like engine soot.

The dependence of hygroscopic growth factor on relative humidity was investigated for H_2SO_4-coated soot generated by the three different fuels, as illustrated in Figure 3-6. For all three soot types, the hygroscopic growth at RH < 50% was negligible. Particles started to take up water at RH between 50% and 60%, depending on the soot type. The hygroscopic growth curves were slightly different for the three types of

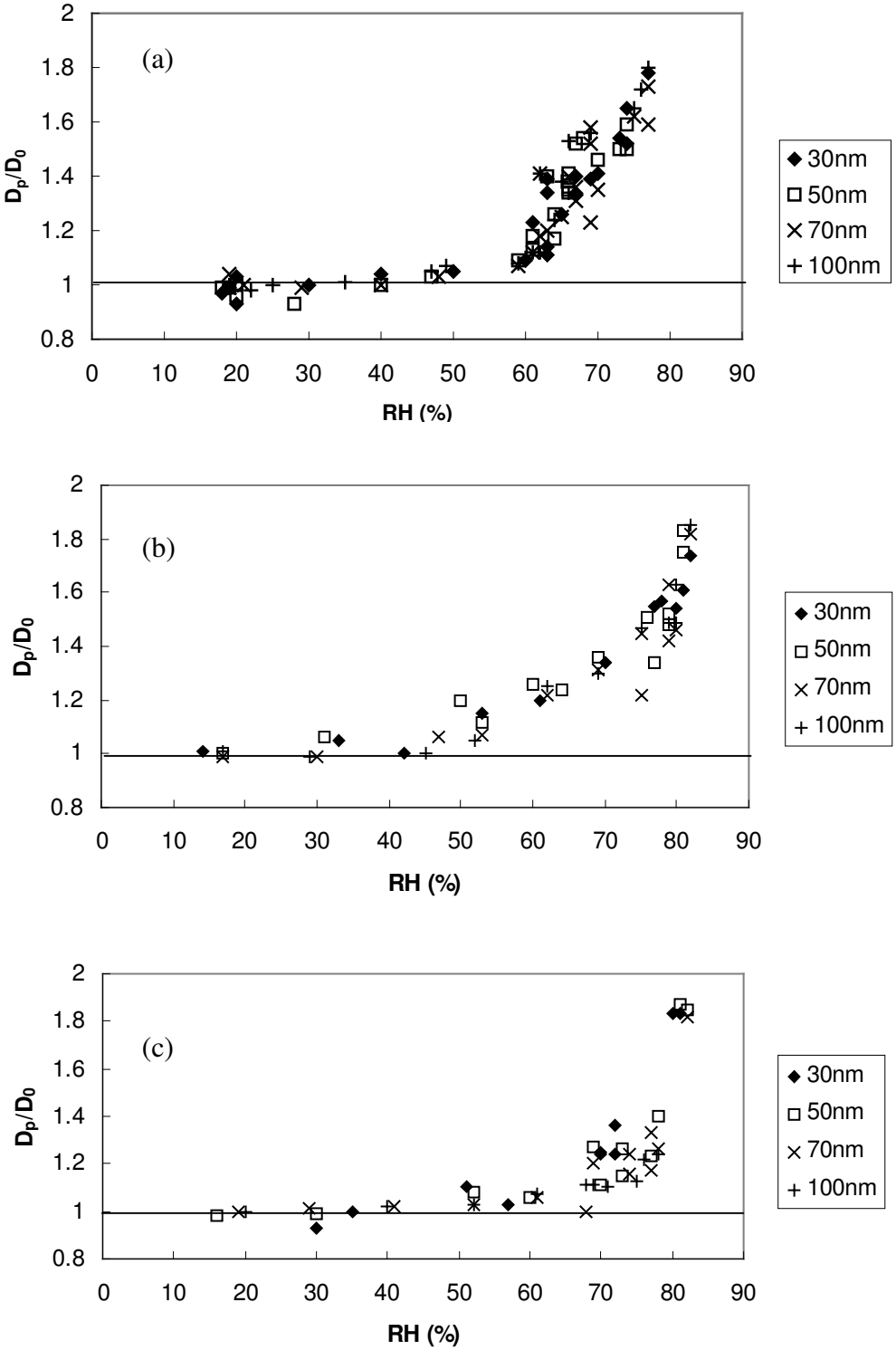

Figure 3-6. Hygroscopic growth factor of H_2SO_4-coated (a) propane (b) methane and (c) kerosene soot aerosols of selected dry particle sizes as a function of RH.

internally mixed soot particles. The growth factor started to increase significantly for propane soot at 60% RH and about 75% RH for kerosene soot. For methane soot, the increase of hygroscopic growth factor was rather smooth between 50% and 80%. At 80% RH, the growth factors for all three types of soot converged at around 1.8, approaching the theoretical growth factor for a pure H_2SO_4 aerosol. Figure 3-7 shows a comparison of the hygroscopic growth curves for the three types of H_2SO_4-coated soot particles. The growth factors at different sizes were not distinguished for each soot type since no clear size dependence was observed.

Previous hygroscopic studies on engine soot indicated much smaller growth factors, ranging from 1.02 to 1.1 at 90% RH for diesel and jet engines soot from sulfur-containing fuels [*Gysel et al.*, 2003; *Weingartner et al.*, 1997]. This is due to the much thinner coating of sulfuric acid and other water soluble components on soot from the combustion process. However, fresh soot in the atmosphere readily undergoes aging processes by adsorbing and condensing gaseous organic and inorganic species as well as incorporating into existing aerosols, resulting in particles with large fractions of soluble components similar to the cases in this study.

Using the measured hygroscopic growth factors at subsaturated conditions, we performed calculations to estimate the Köhler curves for the H_2SO_4-coated soot particles at various sizes. The calculated Köhler curves with dry particle diameters ranging from 30 nm to 100 nm are shown in Figure 3-8. The predicted critical supersaturation values for cloud droplet activation are 0.67%, 0.32% 0.20%, and 0.12% for dry particle sizes of 30 nm, 50 nm, 70 nm, and 100 nm, respectively. Additional CCN measurements using

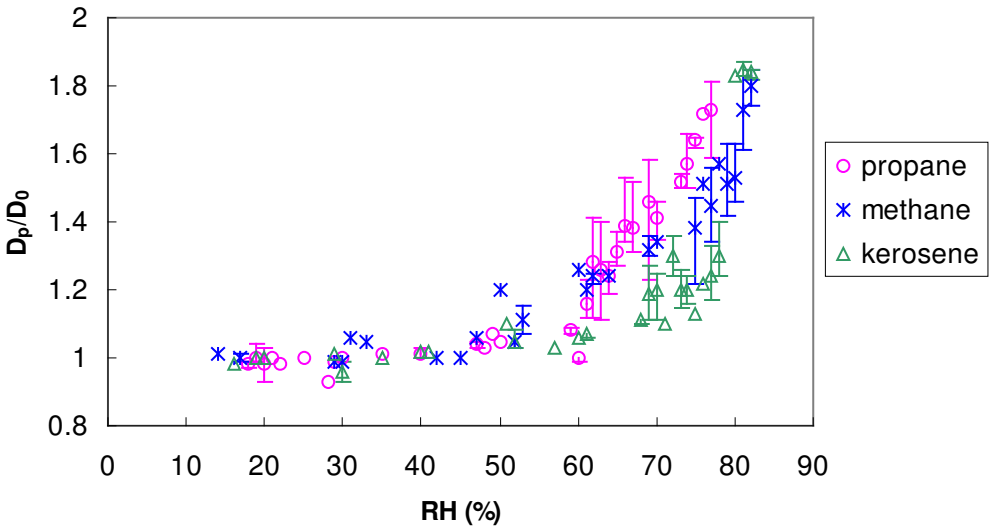

Figure 3-7. Comparison of hygroscopic growth factors of three types of H_2SO_4-coated soot aerosols. Error bars indicate the scatter of experimental data.

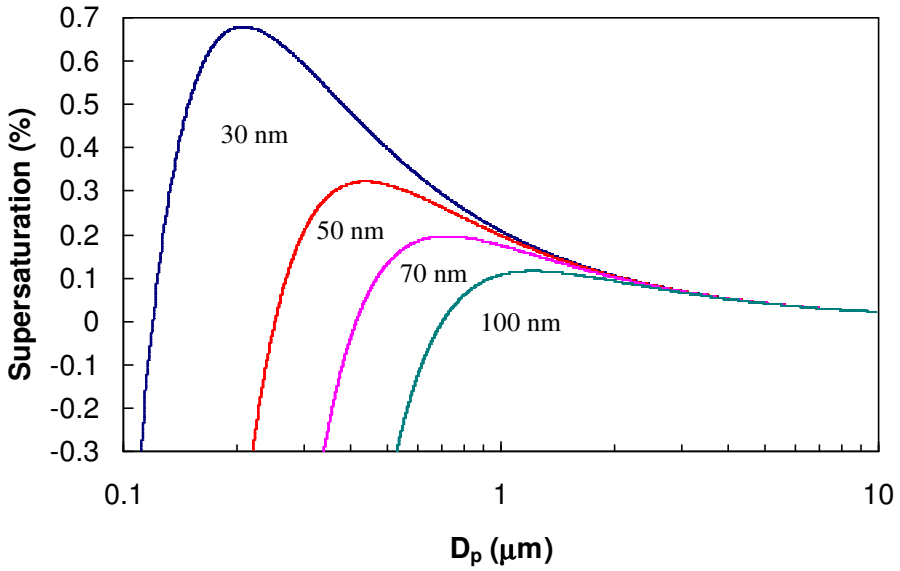

Figure 3-8. Calculated Köhler curves for H_2SO_4-coated soot particles of various sizes using the measured hygroscopic growth factors.

the CCN counter were conducted for fresh and H_2SO_4-coated soot at various supersaturations (ss) between 0.15% and 0.4%. Fresh soot showed no evidence of activation up to 0.4% ss. For H_2SO_4-coated soot produced under similar conditions in the hygroscopic experiments, significant activation was observed. The averaged activation sizes were between 120 nm and 60 nm for the range of 0.15% to 0.4% ss, suggesting that the coated soot particles can readily activate into cloud droplets in the atmosphere. The measured and calculated critical supersaturations for a given particle diameter agree within 50%, with the calculated values typically smaller than the measured ones. The discrepancy is likely due to the overestimation of the particle diameter by DMA due to the fractal structure of soot.

In the present experiments, the flame soot was exposed to H_2SO_4 to acquire an internal coating by passing through a H_2SO_4 reservoir consisting of a 96 wt % solution at room temperature. The residence time of the soot-laden flow in the H_2SO_4 reservoir was estimated to be about a few seconds. The vapor concentration of the 96 wt % H_2SO_4 at 298 K is about 6×10^{11} molecule cm^{-3}, while the ambient vapor concentration of sulfuric acid is on the order of 10^7 molecule cm^{-3} [*Zhang et al.*, 1993a; *Zhang et al.*, 1993b]. Hence to achieve a H_2SO_4 coating characteristic of our present experiments would require a time scale on the order of a few days under the ambient H_2SO_4 concentrations. Our results suggest that aging of freshly produced combustion soot due to adsorption of sulfuric acid significantly alters the hygroscopicity and the cloud-forming potential of soot.

3.4. Summary

Fresh soot particles from fossil fuel combustion, automobile and aircraft emissions and biomass burning are unlikely hygroscopic. However, aging of fresh soot particles in the atmosphere convert them from hydrophobic to hydrophilic aerosols. One important aging pathway is through adsorbing sulfuric acid produced from combustion of sulfur-containing fuels and other atmospheric chemical processes. The results from our experimental study indicate that H_2SO_4-coated soot particles are strongly hygroscopic at subsaturated conditions, impacting their optical and cloud-forming properties. In addition, the hydrophilic soot particles can easily be scavenged by cloud droplets leading to an efficient wet removal and a shortened atmospheric lifetime of soot. The influence of aged soot particles on global radiative transfer, cloud formation, and climate is largely ignored by current global climate models. Better understanding of the soot aging processes is of great importance in further characterizing the direct and indirect effect of soot in the atmosphere.

CHAPTER IV

SCATTERING AND EXTINCTION PROPERTIES OF SOOT-CONTAINING AEROSOLS

4.1. Introduction

Atmospheric aerosols have the potential to perturb the radiation balance of the Earth and therefore to affect the regional and global climate, either directly through scattering and absorption of solar radiation or indirectly by acting as cloud condensation nuclei (CCN). The changes in radiative fluxes induced by aerosols, referred to as aerosol radiative forcing, is an important component of climate forcing that has been the center of attention to atmospheric scientists in recently years [e.g., *IPCC,* 2001; *Rosenfeld*, 2000]. The direct aerosol effect on the solar flux through the atmosphere is determined by the aerosol optical depth, the single scattering albedo, the phase function (in particular the asymmetry factor), and the wavelength dependence of these quantities [*Chylek and Wong*, 1995]. Light absorption in the visible range by airborne particles is primarily due to soot and mineral dust. Hence the optical properties of atmospheric soot and soot-containing aerosols may have direct impacts on atmospheric visibility as well as local and global climate. Knowledge of soot optical properties, including absorption, scattering, extinction, and refractive index, is needed to quantify atmospheric radiative transfer. Currently large uncertainties exist in the reported values of the absorption coefficient of soot [*Liousse et al*., 1993]. The discrepancies are likely attributed to soot morphologies, uncertainties in the complex refractive index of soot, and inaccurate or inconsistent values of material density [*Fuller et al.,* 1999]. Moreover, freshly emitted

soot is subjected to several aging processes in the atmosphere, particularly in industrial regions, such as adsorption and condensation of gaseous species on the soot surface [*Zhang and Zhang*, 2005], coagulation of soot with other pre-existing aerosol constituents [*Kotzick and Niessner*, 1999], and oxidation of soot by various atmospheric species [e.g., *Choi and Leu*, 1998]. Internally mixed soot particles are also produced from burning fuels with sulfur-containing additives.

Several recent field experiments including SCAR-B [*Kaufman et al.,* 1998], TARFOX [*Russell et al.*, 1999], INDOEX [*Ramanathan et al.*, 2001], LACE 98 [*Petzold et al.*, 2002], and SAFARI 2000 [*Eck et al.*, 2003] have been conducted in order to study the optical properties of atmospheric aerosols and to reduce the uncertainties due to aerosol effects in predicting climate change. These field experiments examined thoroughly the optical properties of ambient aerosols, however, they were unable to provide information on the dependence of the aerosol optical properties on chemical composition, size distribution, mixing state, etc. under controlled conditions.

In addition to the field measurements, a number of modeling studies have been carried out to investigate the potential impact of mixing of soot on its optical properties. The model calculations indicated that internal mixture of soot with other aerosol ingredients appears significantly more absorptive than the external mixture counterpart [e.g. *Fuller et al.*, 1999; *Jacobson*, 2000]. Hence current radiative transfer models overestimate the aerosol cooling effect significantly by assuming that atmospheric soot is externally mixed [*Jacobson* 2001]. Because of the high positive forcing of soot mixtures, it was suggested that nearly all of the cooling effect predicted for the external

mixture balances the net cooling effect of other anthropogenic aerosol constituents [*Jacobson*, 2001]. In these model investigations the aerosol optical properties were usually calculated by Mie Theory. While this is applicable for spherical particles such as aqueous sulfate aerosol, fractal-like soot particles makes a reliable modeling of their optical properties much more difficult.

Despite the ample field measurements and modeling studies, little has been done in the laboratory to investigate the impact of mixing with other aerosol species on the optical properties of soot. To date the only available laboratory study was an international soot aerosol characterization experiment conducted in 1999 at the AIDA aerosol chamber in Karlsruhe, Germany [*Saathoff et al.*, 2003b]. One focus of this experiment was on the effect of mixing with other aerosol constituents, such as ammonium sulfate and secondary organic matter, on the optical properties of soot produced from both a diesel vehicle and a spark generator [*Schnaiter et al.*, 2003; *Schnaiter et al.*, 2005a]. It was found that coagulation-induced mixing of soot with ammonium sulfate particles only had a minor effect on the soot absorption cross section, while coatings of organic matter on soot lead to a strong enhancement of both the absorption cross section and the single scattering albedo.

Sulfuric acid vapor in the tropospheric is produced by the oxidation of SO_2, which is from either direct industrial and automobile emission or oxidation of reduced biogenic sulfur compounds. The tropospheric concentration of sulfuric acid vapor is as high as 10^7 molecule cm^{-3} [*Kulmala et al.*, 2000]. Gaseous sulfuric acid plays an important role in atmospheric new particle formation and growth, both *via* homogeneous

nucleation with H_2O, NH_3, or organic vapors [e.g. *Weber et al.*, 1996; *Viisanen et al.*, 1997; *Zhang et al.*, 2004], and heterogeneous scavenging by preexisting aerosols such as soot. Despite the abundance and the climatic impact of soot and H_2SO_4 in the atmosphere, no laboratory study is currently available on the optical properties of soot mixed with sulfuric acid in a controlled manner. In this work, two important optical parameters, the scattering and extinction coefficients of soot are measured dependent on particle size and sulfuric acid coating. The effects of coating and particle size on a number of important parameters, such as the single scattering albedo, the Angström exponent, and the hemispheric backscattering ratio of soot are subsequently evaluated.

4.2. Experimental Section

Three types of aerosols were generated during the experiments including ammonium sulfate, fresh soot, and soot with a sulfuric acid coating. Water solution of ammonium sulfate was nebulized using a commercial atomizer (TSI, Model 3076) to produce "white" aerosols for instrument calibration. Fresh soot aerosols were generated by burning propane using a co-flow laminar diffusion burner as described in Section 3-2. Coating of soot with sulfuric acid was achieved by passing the dry fresh soot stream through a H_2SO_4 reservoir as described in the previous chapter.

The experimental apparatus used for the aerosol scattering and extinction measurements is illustrated in Figure 4-1. The $(NH_4)_2SO_4$ or soot-containing aerosols were entrained into a differential mobility analyzer (DMA) where a certain particle size was selected by applying a fixed high voltage to the DMA. A N_2 dilution flow with ten times the flow rate of the monodisperse aerosol flow was added downstream of the

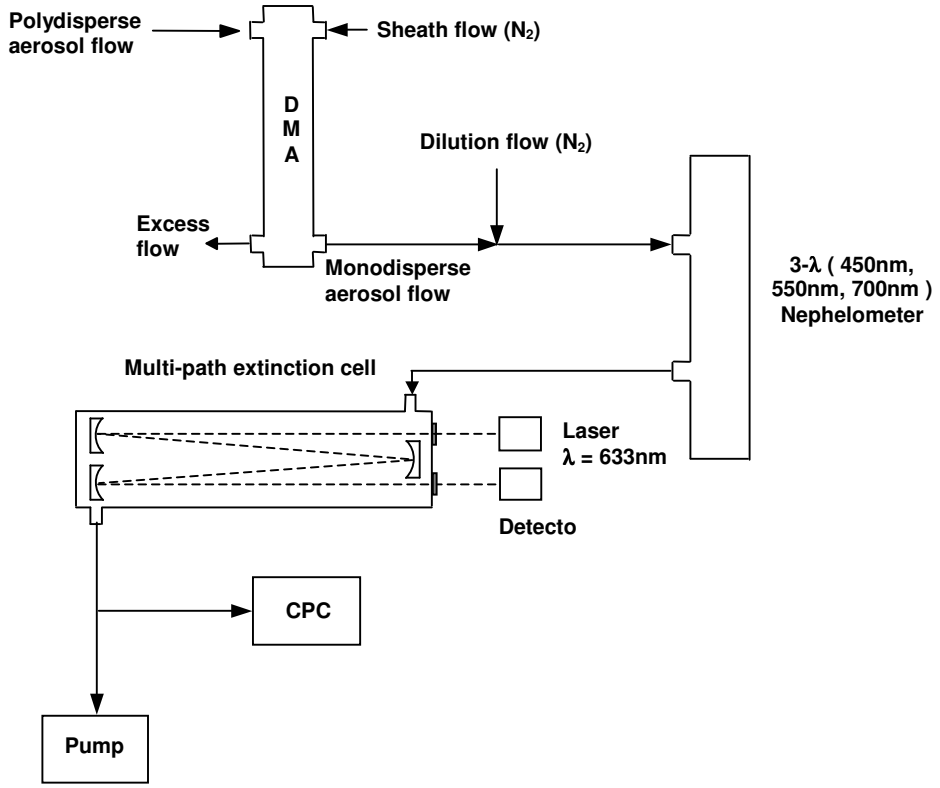

Figure 4-1. Schematic diagram of the experimental apparatus for measurements of aerosol scattering and extinction coefficients.

DMA in order to reduce particle coagulation and wall loss in the optical instruments. The diluted aerosol stream was subsequently introduced into a three-wavelength integrating nephelometer (TSI, Model 3565) to measure the scattering coefficients at 450, 550, and 700 nm. The extinction coefficients were measured using a variable path-length long-path extinction cell (Infrared Analysis, Model 107-V) connected in series with the nephelometer, which had two types of configurations, “White” and “Hanst”, with a maximum path length of 116.6m. A Helium-Neon laser (ThermoOriel, Model 79245) operating at a wavelength of 632.8 nm was employed to provide the incident beam into the extinction cell. The intensity of the transmitted beam after passing through the cell for multiple times was then measured by a photodetector (Newport, Model 818-SL) in conjunction with an optical power meter (Newport, Model 1815-C). The majority of the aerosol flow exiting the extinction cell was discarded through a pump and only a small portion was diverted into a condensation particle counter (CPC, TSI 3760A) to obtain the aerosol number concentration.

The aerosol extinction coefficient was determined by observing the change in transmission of the laser beam when an aerosol flow was present in the extinction cell. During each experimental run, a filtered particle-free airflow was first introduced into the detection system prior to the aerosol optical measurement. The transmitted beam intensity (I_o) was measured as the zero-extinction background under this condition. Monodisperse $(NH_4)_2SO_4$ or soot-containing aerosol flow was then entrained into the extinction cell and the new beam intensity was recorded (I). The light extinction

coefficient b_{ext} in m^{-1} for monochromatic light was related to the light transmittance, I / I_o, via the Beer-Lambert Law,

$$I / I_o = \exp(-b_{ext} L),$$

where L is the total path length in m. The aerosol residence time in the extinction cell was approximately 2 min under typical experimental conditions. At the end of each experiment, the aerosol flow was turned off and a filtered particle-free airflow was again introduced into the optical system to obtain background signals.

The aerosol scattering coefficient was measured directly using the integrating nephelometer. This instrument is widely used to measure the total amount of light scattered by aerosols, covering scattering angles from near forward to near backward, and has been extensively characterized previously [*Anderson et al.*, 1996]. In brief, the aerosol-laden sample flow is introduced into the measurement volume where it is illuminated over an angle of 7 to 170 degrees by a halogen light source. The sample volume is viewed by three photomultiplier tubes (PMTs) through a series of apertures along the axis of the instrument. The light scattered by the aerosols is split into three wavelengths using color filters in front of the PMT detectors. Measurements of the aerosol light scattering signal, the PMT dark current, and the light-source signal are facilitated with a constantly rotating reference chopper. Using the measured scattering coefficients, b_{sca} in m^{-1}, at the three wavelengths, 450, 550, and 700 nm, a spectral dependence of scattering coefficient can be derived following the expression

$$b_{sca} = c\, \lambda^{-\alpha},$$

where α is the Ångström exponent and c is a constant. The scattering coefficients measured by the nephelometer can hence be interpolated to λ = 633 nm using the above relation to match the wavelength of the extinction measurement. The nephelometer also measures hemispheric backscattering coefficients (b_{bck} in m^{-1}) at the three wavelengths, which can be combined with the total scattering to determine the hemispheric backscattering ratio $\beta = b_{bck} / b_{sca}$. The aerosol residence time in the nephelometer was approximately 1 min under typical experimental conditions.

Errors associated with the integrating nephelometer mainly lie in coarse particle (>5 μm) loss at the inlet, droplet evaporation due to heating of the aerosol at high relative humidities, and the truncation of light scattered in the near forward direction (between 0° and 7°). For our experiments of laboratory generated low RH submicron aerosols, the first two errors were minimal. The angular nonidealities were corrected using the methods suggested by *Anderson and Ogren* [1998].

Combining the measured extinction and scattering coefficients, the single scattering albedo (ω) can be determined as the ratio of $b_{sca} / b_{ext,}$ at the wavelength of 633 nm. Experiments were conducted for both fresh and H_2SO_4-coated soot at various mobility diameters to investigate the dependence of ω of soot on particle size and coating.

4.3. Results and Discussions

Prior to the optical measurements of soot-containing aerosols, test runs on laboratory-generated non-absorbing ("white") $(NH_4)_2SO_4$ aerosols were conducted in order to calibrate the nephelometer and the extinction cell. The imaginary part of the

refractive index of $(NH_4)_2SO_4$ in the visible spectrum is very close to zero, thus the absorption is negligible and the scattering and extinction coefficients should agree closely. Figure 4-2 shows the temporal evolution of the measured extinction coefficient at 633 nm, the scattering coefficient at 700 nm directly obtained from the nephelometer, the scattering coefficient interpolated to 633 nm after corrections for angular nonidealities, and CPC particle concentration in an experimental run of $(NH_4)_2SO_4$ aerosols of 250 nm in diameter. For non-absorbing $(NH_4)_2SO_4$, the nephelometer correction factors for angular nonidealities were adopted to be 1.09, 1.07, and 1.05 for 450 nm, 550 nm, and 700 nm, respectively, following the recommendations by *Anderson and Ogren* [1998]. These values agree with the calculated correction factors for highly scattering biomass burning aerosol, with a SSA (λ=700 nm) of 0.8 [*Schnaiter et al.*, 2005b]. In the same study, the authors also suggested that the nephelometer correction was negligible for the highly absorbing soot particles with a SSA (λ=550nm) of 0.2.

Figure 4-2 indicates that the extinction and scattering coefficients correlate well even during an unstable aerosol run. The measured extinction coefficients at 633 nm wavelength agree reasonably well with the scattering coefficients interpolated to 633 nm with corrections for the nephelometer. Such calibration experiments were performed using $(NH_4)_2SO_4$ aerosols of two selected sizes: 200 and 250 nm in diameter, and the comparison of the extinction and scattering coefficients at 633 nm wavelength is illustrated in Figure 4-3. The small differences (3-4%) in the two properties are likely caused by particle loss in the nephelometer, resulting in a slightly smaller extinction than

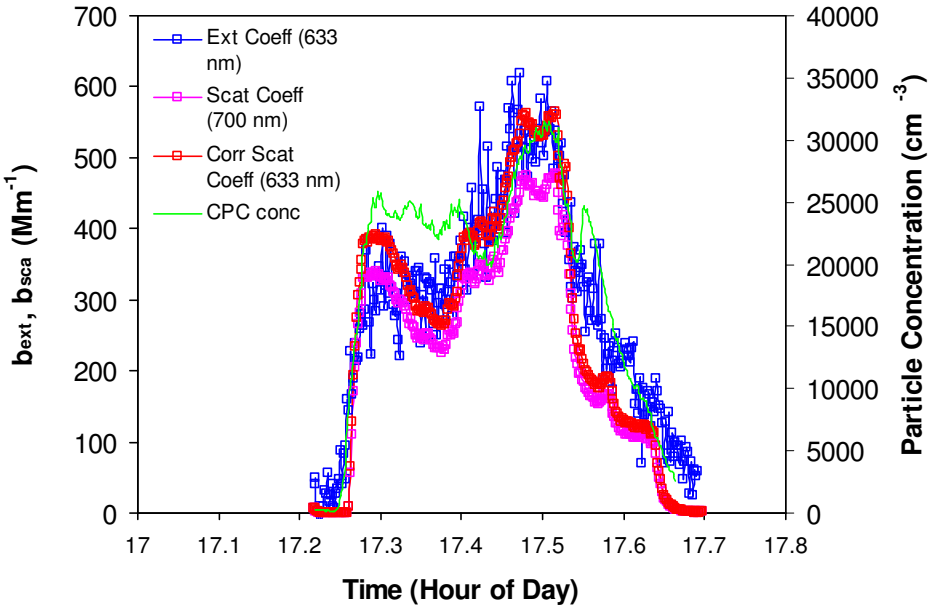

Figure 4-2. Extinction coefficient (633nm), scattering coefficient (700nm), corrected scattering coefficient (633nm), and CPC particle concentration for a white (pure $(NH_4)_2SO_4$) aerosol run, D_p = 250 nm.

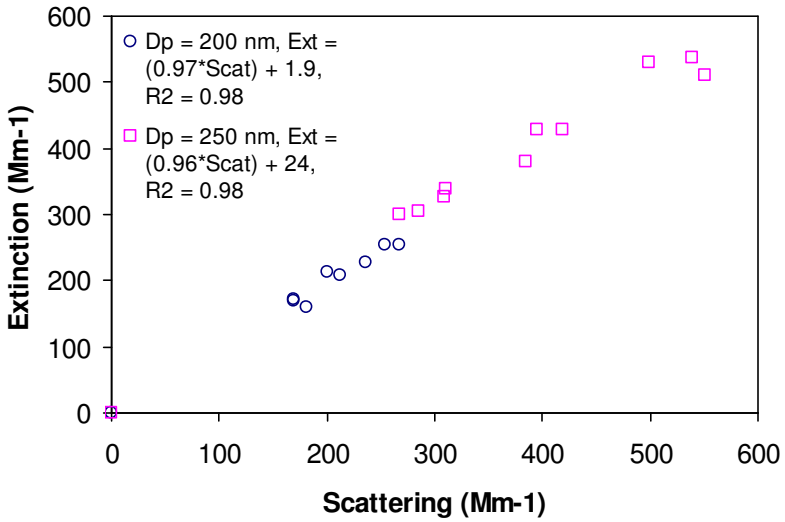

Figure 4-3. Comparison of concurrent extinction and scattering measurements for white (pure $(NH_4)_2SO_4$) aerosol runs.

scattering. In deed, higher extinction was observed when the extinction cell was placed before the nephelometer. Nevertheless, in all the experiments, aerosol flows passed through the nephelometer before the extinction cell because the latter introduced more particle loss due to (1) longer residence time and (2) the location of the aerosol outlet which was behind one of the mirrors.

The scattering and extinction coefficients for both fresh soot and soot with H_2SO_4 coating were measured. During a typical experimental run, the zero-extinction background (I_o) was first measured by passing filtered air through the nephelometer and extinction cell. Then either a fresh or coated soot aerosol stream was introduced into the optical system and the scattering and extinction measurements were conducted concurrently during a period with relatively stable aerosol load. The extinction cell had an estimated detection sensitivity of $10^{-5} – 10^{-4}$ m^{-1}. Typical aerosol concentrations were on the order of $10^4 – 10^5$ cm^{-3}, corresponding to approximately 5-10% transmission loss in laser intensity (I) and $10^{-4} – 10^{-3} m^{-1}$ in extinction coefficient (b_{ext}). For scattering coefficients (b_{sca}) measured at the three wavelengths, 450, 550, and 700 nm, a power law fit was obtained to deduce the Ångström exponent, α, according to $b_{sca} = c\ \lambda^{-\alpha}$, and the derived α and c values are further used to calculate b_{ext} at the wavelength of 633 nm. Corrections were not made for the nephelometer angular truncation because it was suggested that the nephelometer correction was negligible for the highly absorbing soot particles [*Schnaiter et al*., 2005b].

Soot-containing aerosols with various particle sizes between 100 nm and 300 nm were studied. For each selected size, the scattering and extinction coefficients were

measured to determine the single scattering albedo (ω) for both fresh and H_2SO_4-coated soot. Figure 4-4 shows two runs of both fresh and coated soot for the same particle diameter of 100 nm, with the averaged ω values being 0.19 for fresh soot and 0.26 for coated soot. Consistent increase of ω was observed for H_2SO_4-coated soot compared with fresh soot of the same diameter, which is due to the non-absorbing component in the internally mixed particle. In a chamber study where diesel soot was coated with secondary organic matter from α-pinene ozonolysis, it was found that the organic coating significantly increased the single scattering albedo of the soot particles [*Schnaiter et al*., 2003]. The optical measurements indicated that this increase was due to the largely enhanced scattering efficiency by the dielectric coating while the absorption amplification by the coating was small. In this study, although the scattering and extinction coefficients were directly measured, in order to compare the absolute change in the scattering and absorption cross sections caused by coating requires precise knowledge of the particle concentrations. However, the particle concentrations measured by the CPC had a rather high uncertainty in this work because of two reasons: first, particle loss in the nephelometer and extinction cell was non-negligible, especially for coated soot containing sticky sulfuric acid; second, high particle concentrations were used due to the relatively low detection sensitivity of the extinction cell, and were approaching the CPC detection limit. Hence only the relative quantity, ω, is used for comparison in this work.

Figure 4-5 shows another two measurements of fresh and coated soot for the particle diameter of 200 nm. Distinct increase in single scattering albedo is observed

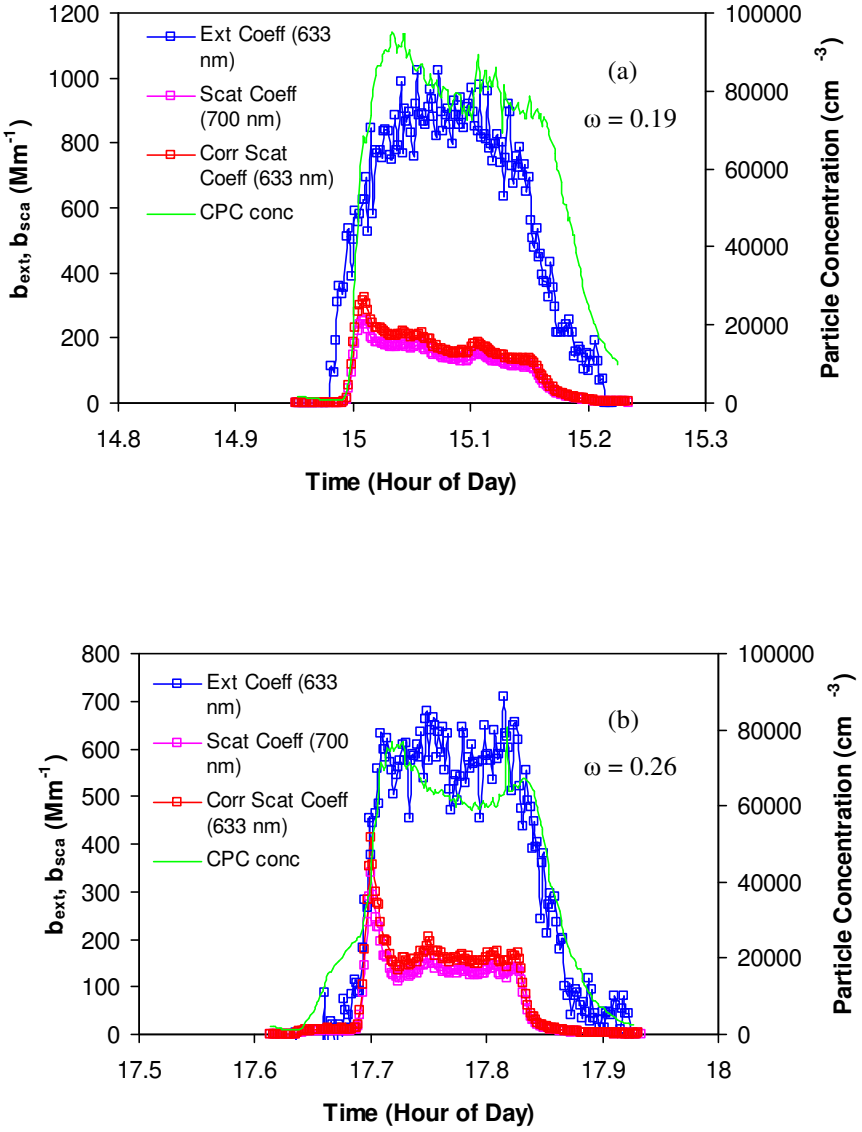

Figure 4-4. Extinction coefficient (633nm), scattering coefficient (700nm), corrected scattering coefficient (633nm), and CPC particle concentration for (a) fresh soot, and (b) H_2SO_4-coated soot with the particle diameter of 100 nm.

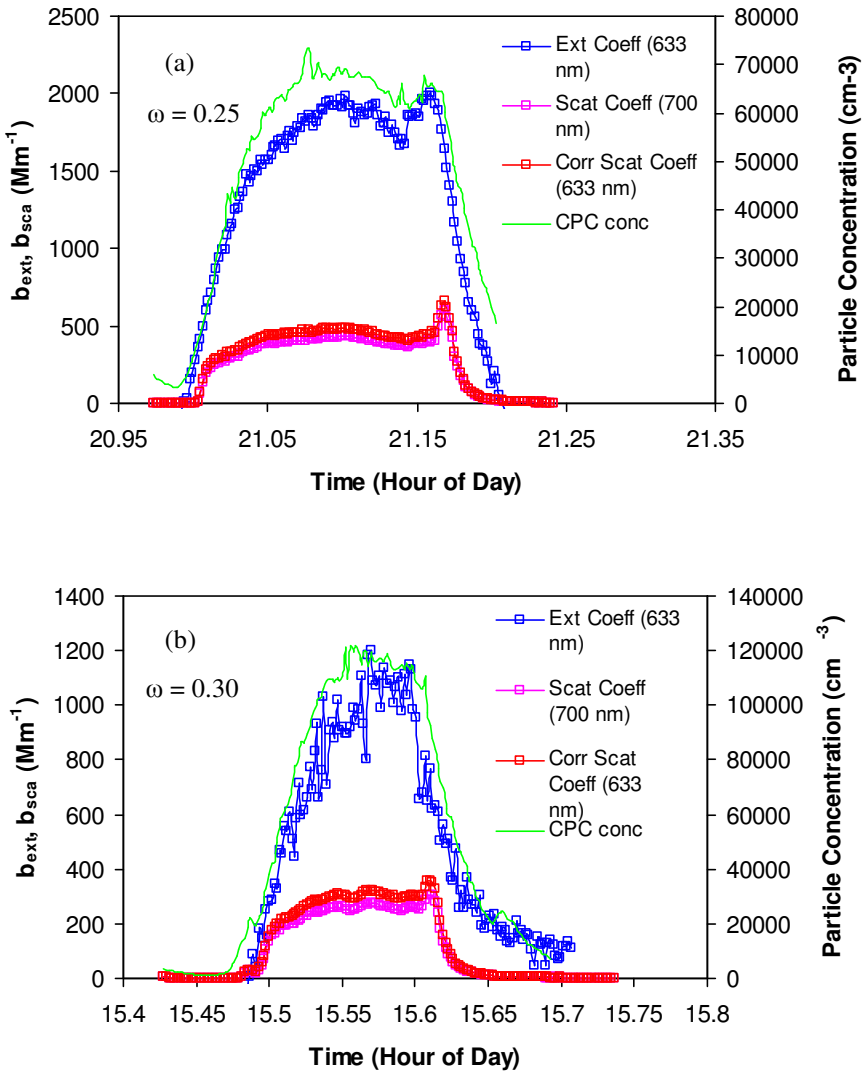

Figure 4-5. Extinction coefficient (633nm), scattering coefficient (700nm), corrected scattering coefficient (633nm), and CPC particle concentration for (a) fresh soot, and (b) H_2SO_4-coated soot with the particle diameter of 200 nm.

with respect to particle size compared with 100 nm particles. The averaged ω values are 0.25 for fresh soot and 0.30 for coated soot for the two experiments in Figure 4-5. There is again an enhancement of ω by the H_2SO_4 coating. All measured single scattering albedo values for both fresh and coated soot at various sizes are summarized in Figure 4-6. For fresh soot, ω increases from 0.18-0.21 for D_p = 100 nm to 0.40 for D_p = 300 nm. A previous laboratory study reported single scattering albedo for soot particles generated from various fuels [*Colbeck et al*., 1997]. The ω value at 632 nm wavelength ranged from 0.24 to 0.31 for hydrocarbon fuels including diesel. In the AIDA soot aerosol study, diesel soot was found to have a ω of about 0.17-0.23 at wavelengths of 450, 550, and 700 nm [*Schnaiter et al*., 2003]. The reported ω values in the above experimental studies are not size-resolved and represent a broad particle size distribution. A modeling study predicted strong size dependence of soot single scattering albedo, which ranges from 0.2 for 100 nm diameter to 0.45 for 300 nm diameter with incident wavelength of 550 nm [*Fuller et al*., 1999]. Our measured size-dependent ω for fresh propane soot agree reasonably well with previous experimental and modeling results. Figure 4-6 also indicates a consistent increase of ω caused by H_2SO_4 coating at various particle sizes.

The Ångström exponent (α) for scattering and the hemispheric backscattering ratio (β) were calculated for all experimental runs using the measured total and back scattering coefficients at the three nephelometer wavelengths. Figure 4-7 illustrates the time evolutions of α and three βs at the three wavelengths corresponding to the two experiments for fresh and coated soot shown in Figure 4-4. In Figure 4-4(b), the scattering is rather stable for the time period with aerosol flow, resulting in a relatively

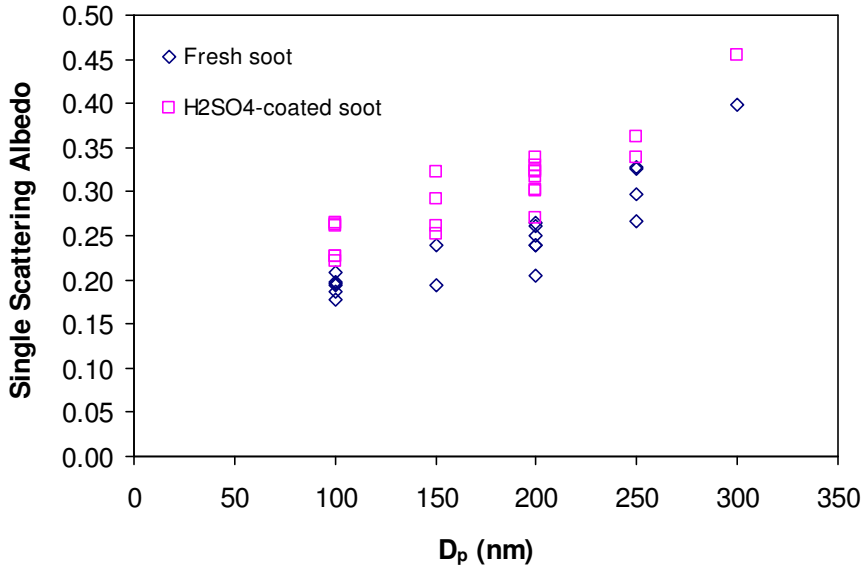

Figure 4-6. Summary of measured single scattering albedo for fresh and H_2SO_4-coated soot at various particle sizes.

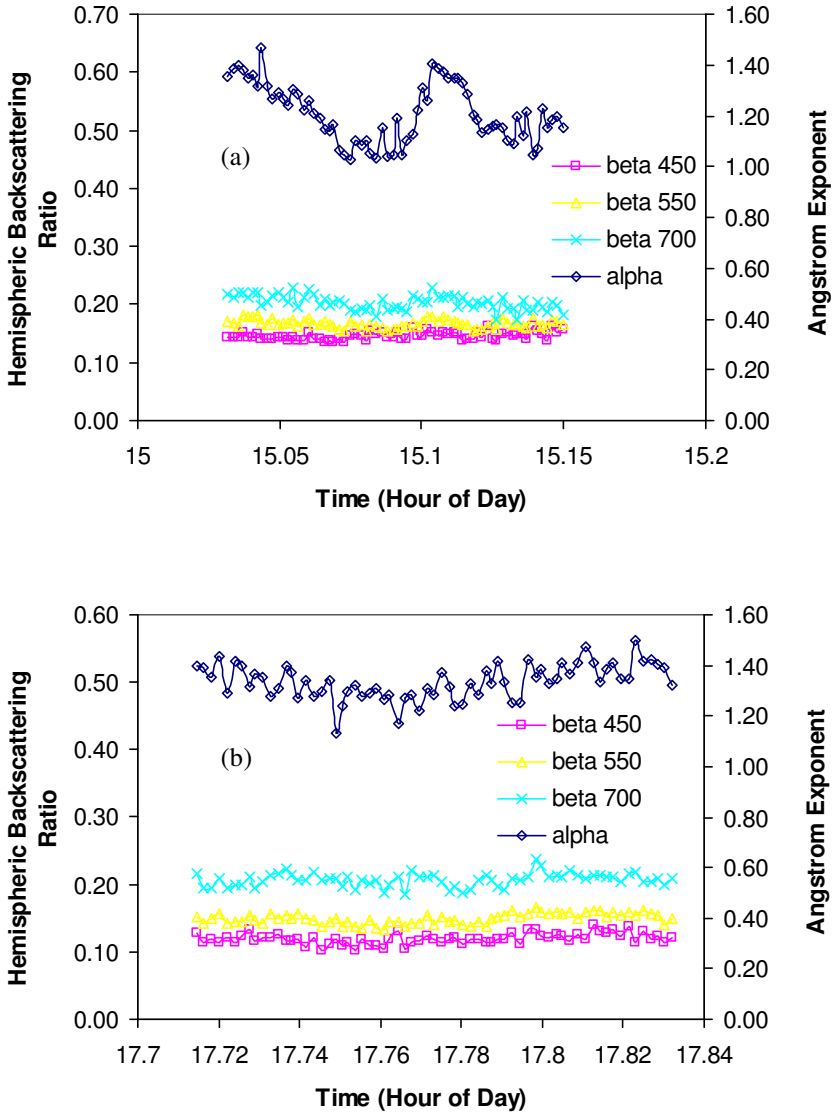

Figure 4-7. Ångström exponent and hemispheric backscattering ratio for the aerosol runs illustrated in Figures 4-4.

stable Ångström exponent profile. In contrast, the variation of α shown in Figure 4-7(a) corresponds to the less stable aerosol run in Figure 4-4(a). Similar correlation of stability between the scattering coefficient and α was also observed in an optical instrument intercomparison experiment [*Sheridan et al*., 2005]. The backscattering ratio seems unaffected by the instability of aerosol flows. In the AIDA experiment for soot with secondary organic coating, both α and β values were found to decrease with increasing amount of coating, with α changing from 2 to 1 and β from 0.18-0.25 to ~ 0.1 during the 25 hr coating period [*Schnaiter et al.,* 2005a]. This change was attributed to the soot particle growth by acquiring an organic coating. The Ångström wavelength exponent is an important parameter in the spectral measurements of both ground-based sunphotometers and satellite remote sensing retrievals, and is commonly used to characterize the wavelength dependence and to provide some basic information on the aerosol size distribution. In this work, α varies from 1.1 to 1.5 for all soot-containing aerosol measurements with no clear dependence on particle size or coating. β is fairly consistent for all soot runs, with values of 0.12-0.14 at λ = 450 nm, 0.14-0.17 at λ = 550 nm, and 0.20-0.23 at λ = 700 nm. The reason for the observed lack of dependence for α and β on particle size is currently unknown. However, the spectral dependence of β is apparent in this study, with increasing β at larger wavelengths. Since the backscattering behavior relies on the size parameter $x = \pi D_p/\lambda$, in the red spectral range particles with the same diameter have a smaller size parameter compared with blue wavelengths, hence less forward scatter and larger β value.

Several uncertainties are associated with the present optical measurements. Particle loss in the nephelometer is estimated to be less than 5% based on the $(NH_4)_2SO_4$ calibration experiments. The loss can be larger in the extinction cell due to longer residence time. Also, aerosols containing H_2SO_4 may be more prone to wall loss. Another source of error in the extinction measured is related to laser stability. The drift in laser intensity is usually less than 0.5% on the experimental time scale. Compared with the typical 5-10% laser intensity loss caused by aerosol extinction, we estimate an error up to 10% in the extinction coefficient associated with laser stability. An additional systematic error is related to the mobility diameter determined by the DMA. For aerosols with fractal structures, such as soot, the mobility diameter is larger than the geometric equivalent diameter [*DeCarlo et al.*, 2005]. This error is smaller for soot with H_2SO_4 coating, since the liquid coating can cause the fractal structure to collapse leading to more spherical aerosol shape.

4.4. Summary

Freshly emitted soot particles readily adsorb gaseous atmospheric constituents, such as sulfuric acid and secondary organic vapors, particularly in polluted areas. Coatings of non-absorbing materials on soot can change its scattering and absorbing efficiencies dramatically. Previous laboratory and modeling studies found that both absorption and scattering efficiencies of soot were greatly enhanced by a non-absorbing coating. Modeling work also suggested that the internal mixture of soot with non-absorbing aerosols exhibited higher positive radiative forcing compared with the external mixture. In our current study, we find that the single scattering albedo of soot is

noticeably enhanced by the sulfuric acid coating. Since the light absorption by soot will not decrease with coating, the increased SSA is caused by scattering enhancement from sulfuric acid, which is predominantly forward scattering for ambient aerosol sizes. This implies that when atmospheric soot actively adsorbs sulfuric acid vapor on its surface, the coated aerosol transfers more solar influx to the atmosphere, leading to an enhanced soot radiative effect compared with fresh soot and gaseous sulfuric acid.

Continuation of the current work includes determining the effects of coating on the scattering and extinction cross sections, in order to validate the previous laboratory and modeling results. This will be facilitated by constructing a high-sensitivity cavity ring-down spectrometer for the extinction measurement, so that particle loss due to high number concentration and long residence time can be minimized, and accurate particle concentration can be obtained. In addition, the RH-dependence of the optical properties will be studied which provides valuable information in determining the soot radiative forcings under ambient conditions. Optical measurements for external mixtures of soot and sulfuric acid aerosols in addition to internal mixtures will also be attempted to evaluate the effects of mixing state on soot radiative effects.

CHAPTER V

SUMMARY

Soot particles released from fossil fuel combustion and biomass burning have a large impact on the regional/global climate by altering the atmospheric radiative properties and by serving as cloud condensation nuclei (CCN). Freshly emitted soot particles are unlikely hygroscopic. However, aging of fresh soot particles in the atmosphere convert them from hydrophobic to hydrophilic aerosols. One important aging pathway is through adsorbing sulfuric acid produced from combustion of sulfur-containing fuels and other atmospheric chemical processes. In this work, experimental studies have been carried out focusing on three integral parts involving the aging of soot by sulfuric acid: (1) heterogeneous uptake of H_2SO_4 on soot; (2) hygroscopic growth of H_2SO_4-coated soot aerosols; (3) effect of H_2SO_4 coating on the scattering and extinction properties of soot particles.

The uptake of H_2SO_4 loss on soot was found to be irreversible, with significant uptake coefficients compared with the uptake of other inorganic atmospheric species (such as HNO_3 or NO_2) on soot. The results imply that the heterogeneous reactions between soot and sulfuric acid proceed efficiently and that the activation of soot by H_2SO_4 represents an important way to facilitate water uptake on soot surface, which is verified by subsequent hygroscopic experiments. The results from our hygroscopic experiments indicate that H_2SO_4-coated soot particles are strongly hygroscopic at subsaturated conditions, having potential impacts on their cloud-forming and optical properties. In addition, the hydrophilic soot particles can easily be scavenged by cloud

droplets leading to an efficient wet removal and a shortened atmospheric lifetime of soot. In our optical study of soot-containing aerosols, it is found that the single scattering albedo of soot is noticeably enhanced by the sulfuric acid coating. Since the light absorption by soot will not decrease with coating, the increased SSA is caused by scattering enhancement from sulfuric acid, which is predominantly forward scattering for ambient aerosol sizes. This implies that when atmospheric soot actively adsorbs sulfuric acid vapor on its surface, the coated aerosol transfers more solar influx to the atmosphere, leading to an enhanced soot radiative effect compared with fresh soot and gaseous sulfuric acid.

The influence of aged soot particles on global radiative transfer, cloud formation, and climate is largely ignored by current global climate models. This work provides critical information concerning the heterogeneous interaction of soot and sulfuric acid, and how their mixing affects the hygroscopic and optical properties of soot. The results will improve our ability to model and assess the soot direct and indirect forcing and hence enhance our understanding of the impact of anthropogenic activities on the climate.

REFERENCES

Ackeman, A. S., O. B. Toon, D. E. Stevens, A. J. Heymsfield, V. Ramanathan, and E. J. Welton (2000), Reduction of tropical cloudiness by soot, *Science*, *288*, 1042-1047.

Akhter, M. S., A. R. Chughtai, and D. M. Smith (1985a), The structure of hexane soot-I: Spectroscopic studies, *Appl. Spect., 39*, 143-153.

Akhter, M. S., A. R. Chughtai, and D. M. Smith (1985b), The structure of hexane soot-II: Extraction studies, *Appl. Spect., 39*, 154-167.

Al-Abadleh, H. A., and V. H. Grassian (2000), Heterogeneous reaction of NO_2 on hexane soot: A Knudsen cell and FT-IR study, *J. Phys. Chem. A*., *104*, 11926-11933.

Alcala-Jornod, C., and M. J. Rossi (2004), Chemical kinetics of the interaction of H_2O vapor with soot in the range 190 K ≤ T ≥ 300 K: A diffusion tube study, *J. Phys. Chem. A.*, *108*, 10667-10680.

Anderson, T. L., D. S. Covert, S. F. Marshall, M. L. Laucks, R. J. Charlson, A. P. Waggoner, J. A. Ogren, R. Caldow, R. L. Holm, F. R. Quant, G. J. Sem, A. Wiedensohler, N. A. Ahlquist, and T. S. Bates (1996), Performance characteristics of a high-sensitivity, three-wavelength, total scatter/backscatter nephelometer, *J. Atmos. Oceanic Technol., 13*, 967-986.

Anderson, T. L., and J. A. Ogren (1998), Determining aerosol radiative properties using the TSI 3563 integrating nephelometer, *Aerosol Sci. Technol., 29,* 57-69.

Aubin, D. G., and J. P. Abbatt (2003), Adsorption of gas-phase nitric acid to n-hexane soot: Thermodynamics and mechanism, *J. Phys. Chem. A., 107*, 11030-11037.

Breon, F. M., D. Tanre, and S. Generoso (2002), Aerosol effect on cloud droplet size monitored from satellite, *Science*, *295*, 834-838.

Brown, R. C., R. C. Miake-Lye, M. R. Anderson, C. E. Kolb, and T. J. Resch (1996), Aerosol dynamics in near-field aircraft plumes, *J. Geophys. Res., 101*, 22939-22953.

Brown, R. L. (1978), Tubular flow reactions with first-order kinetics, *J. Res. Natl. Bur. Stand. (U. S.)., 83*, 1-8.

Choi, W., and M. T. Leu (1998), Nitric acid uptake and decomposition on black carbon (soot) surfaces: Its implications for the upper troposphere and lower stratosphere, *J. Phys. Chem. A., 102*, 7618-7630.

Chylek, P., and J. Wong (1995), Effect of absorbing aerosols on global radiation budget, *Geophys. Res. Letts*., 22, 929-931.

Colbeck, B. Atkinson and Y. Johar (1997), The morphology and optical properties of soot produced by different fuels, *J. Aerosol Sci., 28*, 715-723.

DeCarlo, P. F., J. G. Slowik, D. R. Worsnop, P. Davidovits, and J. L. Jimenez (2005), Particle morphology and density characterization by combined mobility and aerodynamic diameter measurements. Part 1: Theory, *Aerosol Sci. Technol., 39*, 184-184.

Eck, T. F., B. N. Holben, D. E. Ward, M. M. Mukelabai, O. Dubovik, A. Smirnov, J. S. Schafer, N. C. Ilsu, S. J. Piketh, A. Queface, J. Le Roux, and R. J. Swap (2003), Variability of biomass burning aerosol optical characteristics in Southern Africa during the SAFARI (2000) dry season campaign and a comparison of single

scattering albedo estimates from radiometric measurements. *J. Geophys. Res. Atmos.*, *108*, Art. No. 8477.

Fenter, F., F. Caloz, and M. J. Rossi (1996), Heterogeneous kinetics of N_2O_5 uptake on salt, with a systematic study of the role of surface presentation (for N_2O_5 and HNO_3), *J. Phys. Chem.*, *100*, 1008-1019.

Ferry, D., J. Suzanne, S. Nitsche, O. B. Popovitcheva, and N. K. Shonija (2002), Water adsorption and dynamics on kerosene soot under atmospheric conditions, *J. Geophy. Res.*, *107*, Art. No. 4734.

Fortner, E. C., J. Zhao, and R. Zhang (2004), Development of ion drift-chemical ionization mass spectrometry, *Anal. Chem.*, *76*, 5436-5440.

Fuller, K. A., W. C. Malm, and S. M. Kreidenweis (1999), Effects of mixing on extinction by carbonaceous particles, *J. Geophys. Res., 104*, 15941-15954.

Gasparini, R., R. Li, and D. R. Collins (2004), Integration of size distributions and size-resolved hygroscopicity measured during the Houston Supersite for compositional categorization of the aerosol, *Atmos. Environ.*, *38*, 3285-3303.

Gysel, M., S. Nyeki, E. Weingartner, U. Baltensperger, H. Giebl, R. Hitzenberger, A. Petzold, and C. W. Wilson (2003), Properties of jet engine combustion particles during the PartEmis experiment: Hygroscopicity at subsaturated conditions, *Geophys. Res. Letts.*, *30*, Art. No. 1566.

Hagen, D. E., M. B. Tureblood, and P. D. Whitefield (1992), A field sampling of jet exhaust aerosols, *Particulate Sci. Technol*, *10*, 53-63.

Hallett, J., J. G. Hudson, and C. F. Rogers (1989), Characterization of combustion aerosols for haze and cloud formation, *Aerosol Sci. Technol.*, *10*, 70-83.

Hanson, D. R., and F. Eisele (2000), Diffusion of H_2SO_4 in humidified nitrogen: Hydrated H_2SO_4, *J. Phys. Chem. A., 104*, 1715-1719.

Hasegawa, S., and S. Ohta (2002), Some measurements of the mixing state of soot-containing particles at urban and non-urban sites, *Atmos. Environ.*, *36*, 3899-3908.

Horvath, H. (1993), Atmospheric light absorption - a review, *Atmos. Environ., 27A,* 293-317.

Intergovernmental Panel on Climate Change (IPCC) (2001), Climate Change 2001: The Scientific Basis, Contribution of Working Group I to the Third Assessment Report of the IPCC Cambridge University Press, New York.

Jacobson, M. Z. (2000), A physically-based treatment of elemental carbon optics: Implications for global direct forcing of aerosols, *Geophys. Res. Lett., 27*, 217-220.

Jacobson, M. Z. (2001), Strong radiative heating due to the mixing state of black carbon in the atmospheric aerosols, *Nature*, *409*, 695-697.

Jefferson, A., F. L. Eisele, P. J. Ziemann, R. J. Weber, J. J. Marti, and P. H. McMurry (1997), Measurements of the H_2SO_4 mass accommodation coefficient onto polydisperse aerosol, *J. Geophys. Res., 102,* 19021-19028.

Jensen, E. J., and O. B. Toon (1997), The potential impact of soot particles from aircraft exhaust on cirrus clouds, *Geophys. Res. Lett*., *24,* 249-252.

Karcher, B., T. Peter, U. M. Biermann, and U. Schumann (1996), The initial composition of jet condensation trails, *J. Atmos. Sci*., *53*, 3066-3083.

Kasper, M., K. Siegmann, and K. Sattler (1997), Evaluation of an *in situ* sampling probe for its accuracy in determining particle size distributions from flames, *J. Aerosol Sci.*, *28,* 1569-1578.

Kaufman, Y. J., P. V. Hobbs, V. W. J. H. Kirchhoff, P. Artaxo, L. A. Remer, B. N. Holben, M. D. King, D. E. Ward, E. M. Prins, K. M. Longo, L. F. Mattos, C. A. Nobre, J. D. Spinhirne, Q. Ji, A. M. Thompson, J. F. Gleason, S. A. Christopher, and S. C. Tsay (1998), Smoke, clouds, and radiation—Brazil (SCAR-B) experiment, *J. Geophys. Res. Atmos.*, *103,* 31783–31808.

Keyser, L. F., S. B. Moore, and M. –T. Leu (1991), Surface reaction and pore diffusion in flow-tube reactors, *J. Phys. Chem*., *95*, 5496 – 5502.

Kirchner, U., V. Scheer, and R. Vogt (2000), FTIR spectroscopic investigation of the mechanism and kinetics of the heterogeneous reactions of NO_2 and HNO_3 with soot, *J. Phys. Chem. A.*, *104,* 8908-8915.

Kotzick, R., and R. Niessner (1999), The effects of aging processes on critical supersaturation ratios of ultrafine carbon aerosols, *Atmos. Environ*., *33*, 2669-2677.

Kulmala, M., U. Pirjola, J. M. Makela (2000), Stable sulphate clusters as a source of new atmospheric particles, *Nature, 404*, 66-69.

Lammel, G., and T. Novakov (1995), Water nucleation properties of carbon black and diesel soot particles, *Atmos. Environ.*, *29*, 813-823.

Lelievre, S., Y. Bedjanian, N. Pouvesle, J. L. Delfau, C. Vovelle, and G. Le Bras (2004a), Heterogeneous reaction of ozone with hydrocarbon flame soot, *Phys. Chem. Chem. Phys., 6*, 1181-1191.

Lelievre, S., Y. Bedjanian, G. Laverdet, and G. Le Bras (2004b), Heterogeneous reaction of NO_2 with hydrocarbon flame soot, *J. Phys. Chem. A.*, *104*, 10807-10817.

Lesins, G., P. Chylek, and U. Lohmann (2002), A study of internal and external mixing scenarios and its effect on aerosol optical properties and direct radiative forcing, *J. Geophys. Res., 107*, Art. No. 4094.

Liousse, C., H. Cachier, and S. G. Jennings (1993), Optical and thermal measurements of black carbon aerosol content in different environments – Variation of the specific attenuation cross-section, sigma (sigma), *Atmos. Environ. A, 27*, 1203-1211.

Longfellow, C. A., A. R. Ravishankara, and D. R. Hanson (1999), Reactive uptake on hydrocarbon soot: Focus on NO_2, *J. Geophys. Res., 104,* 13833-13840.

Longfellow, C. A., A. R. Ravishankara, and D. R. Hanson (2000), Reactive and nonreactive uptake on hydrocarbon soot: HNO_3, O_3, and N_2O_5, *J. Geophys. Res.*, *105*, 24345-24350.

Mallet, M., J. C. Roger, S. Despiau, J. P. Putaud, and O. Dubovik (2004), A study of the mixing state of black carbon in urban zone, *J. Geophys. Res., 109*, D04202, doi:10.1029/2003JD003940.

Maricq, M. M., S. J. Harris, and J. J. Szente (2003), Soot size distributions in rich premixed ethylene flames, *Combust. Flame*, *132*, 328-342.

Middlebrook, A. M., L. T. Iraci, L. S. McNeill, B. G. Koehler, M. A. Wilson, O. W. Saastad, M. A. Tolbert, and D. R. Hanson (1993), Fourier transform-infrared studies of thin H_2SO_4/H_2O films – Formation, water uptake, and solid-liquid phase-changes, *J. Geophys. Res*., *98*, 20473-20481.

Okada, K., and J. Heintzenberg (2003), Size distribution, state of mixture and morphology of urban aerosol particles at given electrical mobilities, *J. Aerosol Sci.*, *34*, 1539-1553.

Penner, J. E., H. Eddleman, and T. Novakov (1993), Towards the development of a global inventory for black carbon emissions, *Atmos. Environ.*, *27A,* 1277-1295.

Persiantseva, N. M., O. B. Popovicheva, and N. K. Shonija (2004), Wetting and hydration of insoluble soot particles in the upper troposphere, *J. Environ. Monit.*, *6*, 939-945.

Petzold, A., M. Fiebig, H. Flentje, A. Keil, U. Leiterer, F. Schröder, A. Stifter, M. Wendisch, and P. Wendling (2002), Vertical variability of aerosol properties observed at a continental site during the Lindenberg Aerosol Characterization Experiment (LACE 98), *J. Geophys. Res., 107*, doi 10.1029/2001JD001043.

Pitchford, M., J. G. Hudson, and J. Hallet (1991), Size and critical supersaturation for condensation of jet engine exhaust particles, *J. Geophys. Res.*, *96*, 20787-20793.

Popovitcheva, O. B., N. M. Persiantseva, M. E. Trukhin, G. B. Rulev, N. K. Shonija, Y. Y. Buriko, A. M. Starik, B. Demirdjian, D. Ferry, and J. Suzanne (2000), Experimental characterization of aircraft combustor soot: Microstructure, surface area, porosity and water adsorption, *Phys. Chem. Chem. Phys. 2*, 4421-4426.

Popovitcheva, O. B., M. E. Trukhin, N. M. Persiantseva, and N. K. Shonija (2001), Water adsorption on aircraft-combustor soot under young plume conditions, *Atmos. Environ.*, *35*, 1673-1676.

Popovicheva, O. B., N. M. Persiantseva, E. E. Lukhovitskaya, N. K. Shonija, N. A. Zubareva, B. Demirdjian, D. Ferry, and J. Suzanne (2004), Aircraft engine soot as contrail nuclei, *Geophys. Res. Letts., 31*, Art. No. L11104.

Poschl, U., M. Canagaratna, J. T. Jayne, L. T. Molina, D. R. Worsnop, C. E. Kolb, and M. J. Molina (1998), Mass accommodation coefficient of H_2SO_4 vapor on aqueous sulfuric acid surfaces and gaseous diffusion coefficient of H_2SO_4 in N_2/H_2O, *J. Phys. Chem. A.*, *102*, 10082-10089.

Posfai, M., J. R. Anderson, P. R. Buseck, and H. Sievering (1999), Soot and sulfate aerosol particles in the remote marine troposphere, *J. Geophys. Res.-Atmos. 104,* 21685-21693.

Prince A. P., J. L. Wade, V. H. Grassian, P. D. Kleiber, and M. A. Young (2002), Heterogeneous reactions of soot aerosols with nitrogen dioxide and nitric acid: Atmospheric chamber and Knudsen cell studies, *Atmos. Environ.*, *36*, 5729-5740.

Ramanathan, V., P. J. Crutzen, J. Lelieveld, A. P. Mitra, D. Althausen, J. Anderson, M. O. Andreae, W. Cantrell, G. R. Cass, C. E. Chung, A. D. Clarke, J. A. Coakley, W. D. Collins, W. C. Conant, F. Dulac, J. Heintzenberg, A. J. Heymsfield, B. Holben, S. Howell, J. Hudson, A. Jayaraman, J. T. Kiehl, T. N. Krishnamurti, D. Lubin, G. McFarquhar, T. Novakov, J. A. Ogren, I. A. Podgorny, K. Prather, K. Priestley, J. M. Prospero, P. K. Quinn, K. Rajeev, P. Rasch, S. Rupert, R.

Sadourny, S. K. Satheesh, G. E. Shaw, P. Sheridan, and F. P. J. Valero (2001). Indian Ocean Experiment: An integrated analysis of the climate forcing and effects of the great Indo-Asian haze, *J. Geophys. Res. 106,* 28371–28398.

Rosenfeld, D. (2000), Suppression of rain and snow by urban and industrial air pollution, *Science*, *287*, 1793-1796.

Russell, P. B., J. M. Livingston, P. Hignett, S. Kinne, J. Wong, A. Chien, R. Bergstrom, P. Durkee, and P. V. Hobbs (1999), Aerosol-induced radiative flux changes off the United States mid-Atlantic coast: Comparison of values calculated from Sunphotometer and *in situ* data with those measured by airborne pyranometer. *J. Geophys. Res., 104*, 2289–2307.

Saathoff, H., K. -H. Naumann, M. Schnaiter, W. Schöck, O. Möhler, U. Schurath, E. Weingartner, M. Gysel and U. Baltensperger (2003a), Coating of soot and $(NH_4)_2SO_4$ particles by ozonolysis products of α-pinene, *J. Aerosol, Sci., 34*, 1297-1321.

Saathoff, H., O. Moehler, U. Schurath, S. Kamm, B. Dippel, and D. Mihelcic (2003b), The AIDA soot aerosol characterisation campaign 1999, *J. Aerosol, Sci., 34*, 1277-1296.

Santoro, R. J., H. G. Semerjian, and R. A. Dobbins (1983), Soot particle measurements in diffusion flames, *Combust. Flame.*, *51*, 203-218.

Schnaiter, M., H. Horvath, O. Möhler, K. –H. Naumann, H. Saathoff, and O. W. Schöck (2003), UV-VIS-NIR spectral optical properties of soot and soot-containing aerosols, *J. Aerosol Sci., 34,* 1421-1444.

Schnaiter, M., C. Linke, O. Möhler, K. –H. Naumann, H. Saathoff, R. Wagner, and U. Schurath (2005a), Absorption amplification of black carbon internally mixed with secondary organic aerosol, *J. Geophys. Res., 110*, D19204.

Schnaiter, M., O. Schmid, A. Petzold, L. Fritzsche, K. F. Klein, M. O. Andreae, G. Helas, A. Thielmann, M. Gimmler, O. Möhler, C. Linke, and U. Schurath (2005b), Measurement of wavelength-resolved light absorption by aerosols utilizing a UV-VIS extinction cell, *Aerosol Sci. Technol., 39,* 249-260.

Schumann, U., J. Strom, R. Busen, R. Baumann, K. Gierens, M. Krautstrunk, F. P. Schroder, and J. Stingl (1996), *In situ* observations of particles in jet aircraft exhausts and contrails for different sulfur-containing fuels, *J. Geophys. Res.*, *101*, 6853-6869.

Seisel, S., Y. Lian, T. Keil, M. E. Trukhin, and R. Zellner (2004), Kinetics of the interaction of water vapour with mineral dust and soot surfaces at T = 298 K, *Phys. Chem. Chem. Phys.*, *6*, 1926–1932.

Sheridan, P. J., W. P. Arnott, J. A. Ogren, E. Andrews, D. B. Atkinson, D. S. Covert, H. Moosmüller, A. Petzold, B. Schmid, A. W. Strawa, R. Varma, and A. Virkkula (2005), The Reno aerosol optics study: An evaluation of aerosol absorption measurement methods, *Aerosol Sci. Technol., 39,* 1-16.

ten Brink, H. M. (1998), Reactive uptake of HNO_3 and H_2SO_4 in sea-salt (NaCl) particles, *J. Aerosol Sci., 29*, 57-64.

Tesner, P. A., and S. V. Shurupov (1995), Some physico-chemical parameters of soot formation during pyrolysis of hydrocarbons, *Combust. Sci. Tech.*, *105*, 147-161.

Twomey, S., M. Piepgrass, and T. L. Wolfe (1984), An assessment of the impact of pollution on global cloud albedo, *Tellus*, *36*, 356-366.

Viisanen, Y., M. Kulmala, and A. Laaksonen (1997), Experiments on gas–liquid nucleation of sulfuric acid and water, *J. Chem. Phys.*, *107*, 920-926.

Weber, R. J., J. J. Marti, P. H. McMurry, F. L. Eisele, D. J. Tanner, and A. Jefferson (1996), Measured atmospheric new particle formation rates: Implications for nucleation mechanisms, *Chem. Eng. Commun., 151*, 53-64.

Weingartner, E., U. Baltensperger, and H.Burtscher (1995), Growth and structural change of combustion aerosols at high relative humidity, *Environ. Sci. Technol., 29*, 2982-2986.

Weingartner, E., H. Burtscher, and U. Baltensperger (1997), Hygroscopic properties of carbon and diesel soot particles, *Atmos. Environ*., *31*, 2311-2327.

Weis, D. D., and G. E. Ewing (1996), Infrared spectroscopic signatures of $(NH_4)_2SO_4$ aerosols, *J. Geophys. Res*., *101*, 18709-18720.

Wentzel, M., H. Gorzawski, K. H. Naumann, H. Saathoff, and S. Weinbruch (2003), Transmission electron microscopical and aerosol dynamical characterization of soot aerosols, *J. Aerosol Sci.*, *34*, 1347-1370.

Widmann, J. F., J. C. Yang, T. J. Smith, S. L. Manzello, and G. W. Mulholland (2003), Measurement of the optical extinction coefficients of post-flame soot in the infrared**,** *Combust. Flame*, *134*, 119-129.

Wyslouzil, B. E., K. L. Carleton, D. M. Sonnenfroh, W. T. Rawlins, and S. Arnold (1994), Observation of hydration of single, modified carbon aerosols, *Geophys. Res. Lett.*, *21*, 2107-2110.

Zhang, D., and R. Zhang (2005), Laboratory investigation of heterogeneous interaction of sulfuric acid with soot, *Environ. Sci. Technol*. *39,* 5722-2728.

Zhang, R., P. J. Wooldridge, J. P. D. Abbatt, and M. J. Molina (1993a), Physical chemistry of the H_2SO_4/H_2O binary system at low temperatures: Implications for the stratosphere, *J. Phys. Chem., 97*, 7351-7358.

Zhang, R., P. J. Wooldridge, and M. J. Molina (1993b), Vapor-pressure measurements for the $H_2SO_4/HNO_3/H_2O$ and $H_2SO_4/HCl/H_2O$ systems – Incorporation of stratospheric acids into background sulfate aerosols, *J. Phys. Chem. 97*, 8541-8548.

Zhang, R., J. T. Jayne, and M. J. Molina (1994a), Heterogeneous interactions of $ClONO_2$ and HCl with sulfuric acid tertahydrate: Implications for the stratosphere, *J. Phys. Chem.*, *3*, 867-874.

Zhang, R., M. T. Leu, and L. F. Keyser (1994b), Heterogenous reactions involving $ClONO_2$, HCl, and HOCl on liquid sulfuric acid surfaces, *J. Phys. Chem., 98*, 13563-13574.

Zhang R., I. Suh, J. Zhao, D. Zhang, E. C. Fortner, X. Tie, L. T. Molina, and M. J. Molina (2004), Atmospheric new particle formation enhanced by organic acids, *Science*, *304,* 1487-1490.

Zuberi, B., K. S. Johnson, G. K. Aleks, L. T. Molina, M. J. Molina, and A. Laskin (2005), Hydrophilic properties of aged soot, *Geophys. Res. Letts.*, *32*, Art. No. L01807.

VITA

Name: Dan Zhang

Address: Department of Atmospheric Sciences, Texas A&M University, College Station, TX 77843-3150

Email Address: dzhang@tamu.edu

Education: B.S., Chemistry, Fudan University, China, 1999

M.S., Atmospheric Sciences, Texas A&M University, 2001